Bulletin of Volcanology (2018) 80:44
https://doi.org/10.1007/s00445-018-1221-5

RESEARCH ARTICLE

Eruptive history of Incahuasi, Falso Azufre and El Cóndor Quaternary composite volcanoes, southern Central Andes

Pablo Grosse[1] · Yuji Orihashi[2,3] · Silvina R. Guzmán[4,5] · Hirochika Sumino[6,7] · Keisuke Nagao[6,8]

Received: 14 December 2017 / Accepted: 23 March 2018

Abstract

Volcanoes can stay dormant for much longer than 10 ka and hence many Quaternary volcanoes lacking Holocene activity have the potential to become active. Reconstructing the eruptive histories of these volcanoes is an important first step towards evaluating their long-term eruptive probabilities. The southern Central Volcanic Zone (CVZ) of the Andes at ~ 27° S latitude has a notable concentration of Quaternary volcanoes, several considered potentially active, but most of which are poorly known. We reconstruct the eruptive histories of three of these volcanoes, Incahuasi, Falso Azufre and El Cóndor, on the basis of field and satellite image mapping and unspiked K-Ar geochronology, supported by petrography and whole-rock geochemistry. Incahuasi (volume of 62 ± 6 km^3) comprises a main conical edifice, capped by a summit crater, that was constructed between ~ 1.6 and 0.7 Ma by mostly andesitic lavas at a growth rate of ~ 0.07 km^3/ka. At 0.8–0.7 Ma, activity shifted to the eastern flank, with the emplacement of a trachydacitic lava dome and a trachyandesitic lava field. At 0.35 Ma, a mafic center consisting of overlapping scoria cones and basaltic andesite lava flows was emplaced on the NE flank. Falso Azufre (98 ± 12 km^3) is an arcuate-shaped massif with several vents aligned NW-SE and ENE-WSW. It contains the remnant of a Pliocene andesitic edifice. The bulk of the massif was constructed between ~ 0.9 and 0.5 Ma by andesitic and trachyandesitic lava flows. More recent activity (< 0.4 Ma) consists of andesitic to dacitic flows, coulées and domes restricted to the summit regions and the eastern flank. The average Quaternary growth rate is ~ 0.1 km^3/ka. El Cóndor (109 ± 8 km^3) is a NW-SE elongated massif with two distinct stages of activity. The Pliocene stage consists of andesitic to dacitic rocks. Recent activity (< 0.15 Ma) is among the youngest recorded in the region and consists mainly of trachyandesitic to trachydacitic lava flows. The estimated eruption rate of ~ 0.4 km^3/ka is one of the highest of the CVZ. Incahuasi has the lowest long-term eruptive potential of the three volcanoes. Falso Azufre has an intermediate long-term eruptive potential and a minor felsic phase may be ongoing. El Cóndor has the highest long-term eruptive potential and its main constructive phase may still be ongoing. Most CVZ volcanoes, including Incahuasi and Falso Azufre, have longer lifespans and lower average growth rates compared to volcanoes from other arcs, suggesting a significant difference between the CVZ and other arcs.

Keywords Composite volcano · Eruptive history · Volcano growth rates · Unspiked K-Ar geochronology · Central Volcanic Zone of the Andes

Editorial responsibility: V. Acocella; Deputy Executive Editor: J. Tadeucci

✉ Pablo Grosse
pablogrosse@yahoo.com

[1] CONICET and Fundación Miguel Lillo, Miguel Lillo 251, San Miguel de Tucumán T4000JFE, Tucumán, Argentina

[2] Earthquake Research Institute, The University of Tokyo, Bunkyo, Tokyo 113-0032, Japan

[3] Present address: Global Environment and Disaster Prevention Sciences, Graduate School of Science and Technology, Hirosaki University, 1 Bunkyo-cho, Hirosaki, Aomori 036-8561, Japan

[4] Instituto de Bio y Geociencias del NOA (IBIGEO), UNSa-CONICET, 9 de Julio 14, Rosario de Lerma 4405, Salta, Argentina

[5] Present address: Institute of Earth Sciences Jaume Almera, ICTJA-CSIC, Lluis Sole i Sabaris s/n, 08028 Barcelona, Spain

[6] Geochemical Research Center, Graduate School of Science, The University of Tokyo, Bunkyo, Tokyo 113-0032, Japan

[7] Present address: Department of Basic Science, Graduate School of Arts and Sciences, The University of Tokyo, 3–8–1 Komaba, Meguro–ku, Tokyo 153–8902, Japan

[8] Present address: Division of Polar Earth–System Sciences, KOPRI (Korea Polar Research Institute), 26 Songdomirae–ro, Yeonsu–gu, Incheon 21990, South Korea

Published online: 04 April 2018

Introduction

Many volcanoes in the world with no record of historic activity are considered potentially active based on different criteria (e.g. youthful morphology, geochronology, thermal and/or fumarolic activity, surface deformation, seismic activity) (e.g. de Silva and Francis 1991; Szakács 1994; McNutt 1996; Siebert et al. 2010; Crosweller et al. 2012; Biggs et al. 2014; Carniel 2014; Brown et al. 2015). Evidence of Holocene activity has been the conventional condition to consider a volcano as active (e.g. Szakács 1994; Siebert et al. 2010), but it has become increasingly evident that volcanoes can have repose periods much longer than 10 ka (e.g. Hildreth and Lanphere 1994; Szakács 1994; Davidson and de Silva 2000; Connor et al. 2006) and hence many Quaternary volcanoes lacking Holocene activity have the potential to become active (e.g. Siebert et al. 2010; Crosweller et al. 2012; Loughlin et al. 2015 and references therein). Indeed, Scandone et al. (2016) suggest that a volcano should be considered active while the processes that lead to an eruption (availability of magma and of a pathway to reach the surface) are still operative, thus not limiting the definition to a specific time frame. Reconstructing the eruptive histories of potentially active volcanoes is necessary to understand their past activity and is a first step towards evaluating their long-term eruptive probability.

In the Central Volcanic Zone of the Andes (CVZ; ~15°–28° S latitude), the eruptive histories of most Quaternary volcanoes are not well constrained. This region contains at least 110 Quaternary composite volcanoes (de Silva and Francis 1991; Siebert et al. 2010), but historical eruptions are known at only 14 of these and only five have Holocene absolute ages (Siebert et al. 2010). Of the remaining ~90 Quaternary volcanoes, ~60 are considered Pleistocene and ~30 are considered to have had Holocene activity, mainly based on their youthful morphologies not affected by glaciation (de Silva and Francis 1991; Siebert et al. 2010). However, determining relative ages for volcanoes of this region has proven difficult (e.g. de Silva and Francis 1991; González-Ferrán 1995; Siebert et al. 2010) given the very low erosion rates due to the arid climate (e.g. Karátson et al. 2012). Furthermore, many of these volcanoes show prolonged lifespans, sometimes longer than 1 Ma (e.g. Taapaca, Clavero et al. 2004b; Ollagüe, Vezzoli et al. 2008), and repose periods well over 0.1 Ma (e.g. Aucanquilcha, Klemetti and Grunder 2008; Llullaillaco, Gardeweg et al. 1984; Richards and Villeneuve 2001), thus making the distinction between dormant or extinct volcanoes particularly challenging. Of the >110 Quaternary volcanoes of the CVZ, ~15 have been studied with some detail, whereas the rest are poorly known, their eruptive histories are ill-constrained and their eruptive potentials are uncertain.

In the southern CVZ, the largest concentration of Quaternary volcanism is found along a ~100 km segment of the arc between 26.4° and 27.3° S latitude, around Paso San Francisco (Fig. 1), with ~20 composite volcanoes (Table 1; Fig. 2). Although only one minor historical eruption has been documented (at Ojos del Salado in 1993), eight volcanoes are listed as Holocene by Siebert et al. (2010) (Table 1). In strong contrast, there is a gap of ~90 km to the north without any Quaternary volcanic center along the main arc (Fig. 1), whereas to the south the only occurrence of Quaternary volcanism is the Incapillo caldera and dome complex (Fig. 1). In addition to its unusual abundance, Quaternary volcanism in the Paso San Francisco region shows a particularly complex spatial distribution and relation with regional tectonic structures. Furthermore, the region is located near the southern end of the CVZ, in a transition zone where the Nazca plate changes its subduction angle from ~30° to sub-horizontal towards the south (e.g. Barazangi and Isacks 1976; Cahill and Isacks 1992). Also, this region partially coincides with a low-velocity seismic zone at ~35 to 20 km depth (Bianchi et al. 2013; Ward et al. 2017), interpreted by Ward et al. (2017) as a 12,000 km^3 magma body.

Notwithstanding the intriguing combination of high magma production rate, complex distribution and particular geodynamic location, the Quaternary volcanoes of the Paso San Francisco region lack detailed studies and are known mostly through regional investigations, geological survey maps and a few more specific contributions (see next section). Here, we reconstruct the eruptive histories of three poorly known volcanoes in this region: Incahuasi, Falso Azufre and El Cóndor (Fig. 2), based on detailed field and satellite image mapping, K-Ar geochronology, petrography and whole-rock geochemistry. Our goals are to increase the basic knowledge of these volcanoes, quantify their volumes, lifespans and growth rates and make a preliminary assessment of their eruptive potentials. Although these volcanoes are located in very remote areas and thus imply minimum risk for local populations, reconstruction of their eruptive histories is an initial step towards assessing the hazards that they may pose, and can give insights for similar volcanoes located in more vulnerable areas within the CVZ. Furthermore, by comparing these volcanoes with others from the CVZ and from other arcs, we highlight basic differences in lifespans and growth rates at CVZ volcanoes.

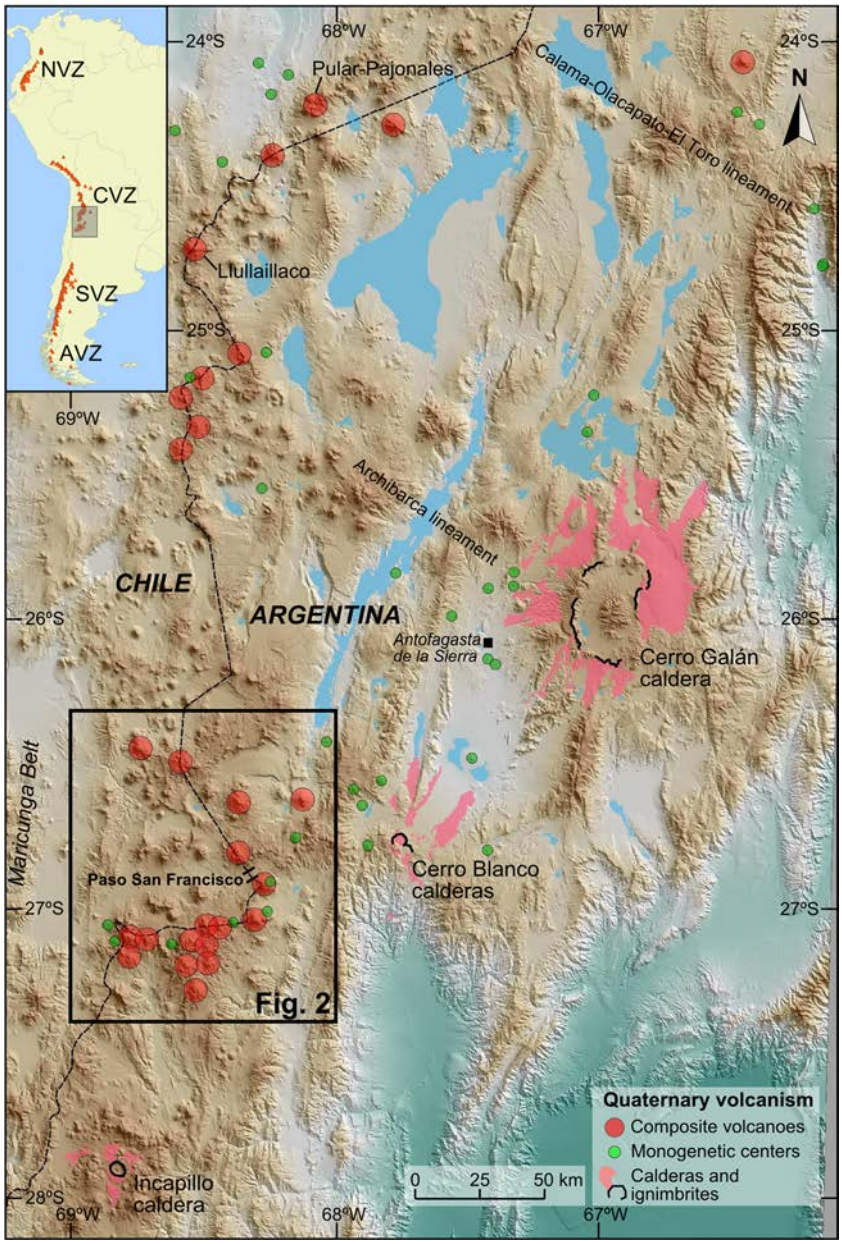

Fig. 1 Location of Quaternary composite volcanoes, monogenetic centers and collapse calderas within the southern Central Volcanic Zone of the Andes draped on Shuttle Radar Topography Mission 90 m digital elevation model-derived shaded relief image. Box indicates extension of Fig. 2. Inset map of South America shows locations of active and potentially active volcanoes (orange triangles) according to Siebert et al. (2010), and the volcanic zones of the Andes (NVZ: Northern Volcanic Zone; CVZ: Central Volcanic Zone; SVZ: Southern Volcanic Zone; AVZ: Austral Volcanic Zone)

Cenozoic volcanism in the Paso San Francisco region

Cenozoic arc volcanism in the southern CVZ began at ca. 26 Ma, in coincidence with the break-up of the Farallon plate into the Nazca and Cocos plates, and an increment in convergence rate between the Nazca and South American plates (e.g. Somoza and Ghidella 2012). In the Paso San Francisco region, between ca. 26 and 8 Ma, the volcanic arc front was located about 60 km west of the present arc front, along the N-S trending Maricunga Belt arc (Fig. 1) (e.g. Mpodozis et al. 1995; Kay and Coira 2009). Only minor backarc activity occurred, first in the Cordillera Claudio Gay (27–21 Ma), and later along the Cordón Los Amarillos (15–12 Ma) (Mpodozis et al. 1996; Clavero et al. 2012; Kay et al. 2014) (Fig. 2). Between ca. 8 and 3 Ma, the arc front migrated eastward to its present position, possibly in response to a major pulse of forearc subduction erosion (Kay and Mpodozis 2002; Kay and Coira 2009; Goss et al. 2013). As a result, numerous Upper Miocene and Pliocene volcanic centers are scattered throughout the Paso San Francisco region, encompasing a broad, ca. 80 km-wide, belt (Fig. 2) (e.g. González-Ferrán et al. 1985; Baker et al. 1987; Mpodozis et al. 1996). During this time, extensive ignimbrite deposits from both recognized

Table 1 List of 20 Quaternary composite volcanoes and lava domes in the Paso San Francisco region of the Central Volcanic Zone of the Andes between 26.4° and 27.3° S latitude. Morphometric data obtained from the Shuttle Radar Topography Mission 30 m digital elevation model using MORVOLC. Entries in italic are distinct edifices or stages within a volcano

Volcano	Latitude (°)	Longitude (°)	Elevation (m)	Height (km)	Exposed area (km^2)	Volume (km^3)	Type[a]	Composition[b]	Age range (Ma)	Activity status[c]	References (ages)[d]
Azufrera-Piedra Parada	−26.452	−68.740	5917	1.4	189	64	Massif	A; D	0.14–9.2	Pleistocene	1, 2
Azufrera de Los Cuyanos					*157*	*36*			*0.14–1.2*		
Piedra Parada					*32*	*27*			*9.2*		
Sierra Nevada	−26.493	−68.560	6140	1.3	285	100	Massif	A; D	0.43–1.7	Holocene	2, 3, 4
Peinado	−26.624	−68.116	5847	1.6	93	20	Cone	BTA; TA	–	Holocene	–
El Cóndor	−26.634	−68.361	6420	1.8	281	109	Massif	TA; A > TD; D	0.02–3.0	Holocene	this study
Cóndor stage					*192*	*41*		*TA > TD*	*0.02–0.13*		
Pre-Cóndor stage					*89*	*68*		*A > D*	*2.7–3.0*		
Cerro Torta	−26.753	−68.140	5460	0.6	14	2.8	Dome	D	0.43	–	5
Falso Azufre	−26.802	−68.362	5897	1.2	387	98	Massif	A; TA > D	0.16–3.5	Holocene?	4, 6, 7, this study
Main Falso Azufre					*356*	*83*		*A; TA > D*	*0.16–0.91*		
Kunstmann edifice					*31*	*15*		*A*	*2.5–3.5*		
Cerro Bertrand	−26.836	−68.163	5266	0.7	111	19	Sub-cone	A	1.1–2.1	–	8
San Francisco	−26.921	−68.263	6031	1.2	94	23	Cone	A; TA	1.0–1.2	Pleistocene	4, 7, our unpublished data
Incahuasi	−27.035	−68.296	6611	2.0	207	62	Cone	A; TA > BTA; TD	0.35–1.6	Holocene?	7, 9, this study
El Fraile	−27.044	−68.381	6052	1.0	22	5.3	Dome	D	0.23; < 1	–	7, 9
El Muertito	−27.064	−68.429	5996	0.7	48	6.2	Cone	A	1.0–1.9	–	9
El Muerto	−27.059	−68.485	6495	1.2	38	12	Cone	D	0.45	–	9
Ojos del Salado	−27.111	−68.541	6874	1.4	148	54	Massif	D	0.34–1.5	Holocene (dated)	7, 9, 10
Medusa	−27.129	−68.485	6127	0.6	53	7.7	Massif	–	–	–	–
El Solo	−27.106	−68.714	6203	0.9	19	4.9	Dome	D	1.3	Holocene	11
Tres Cruces	−27.100	−68.779	6737	1.6	226	83	Massif	D	0.03–4.4	Pleistocene	7, 11
Main Tres Cruces					*126*	*38*			*0.03–2.1*		
Cristi-Rodrigo					*100*	*45*			*2.5–4.4*		
Del Viento	−27.192	−68.474	6012	0.8	58	9.6	Sub-cone	–	–	–	–
Tipas	−27.198	−68.561	6666	1.1	211	52	Massif	–	–	Holocene	–
Olmedo	−27.209	−68.526	6219	0.5	35	2.6	Cone	–	–	–	–
Nacimientos	−27.283	−68.525	6454	1.3	118	36	Sub-cone	–	–	–	–

[a] Following classifications by Grosse et al. (2009, 2017)

[b] *A* andesite, *TA* trachyandesite, *BTA* basaltic trachyandesite, *D* dacite, *TD* trachydacite

[c] According to Siebert et al. (2010)

[d] References: 1: Naranjo and Cornejo (1992); 2: Polanco et al. (2014); 3: Clavero et al. (1997); 4: Clavero et al. (2012); 5: Seggiaro et al. (2006); 6: Zentilli (1974); 7: Mpodozis et al. (1996); 8: Kay et al. (2006); 9: González-Ferrán et al. (1985); 10: Gardeweg et al. (1997); 11: Gardeweg et al. (2000)

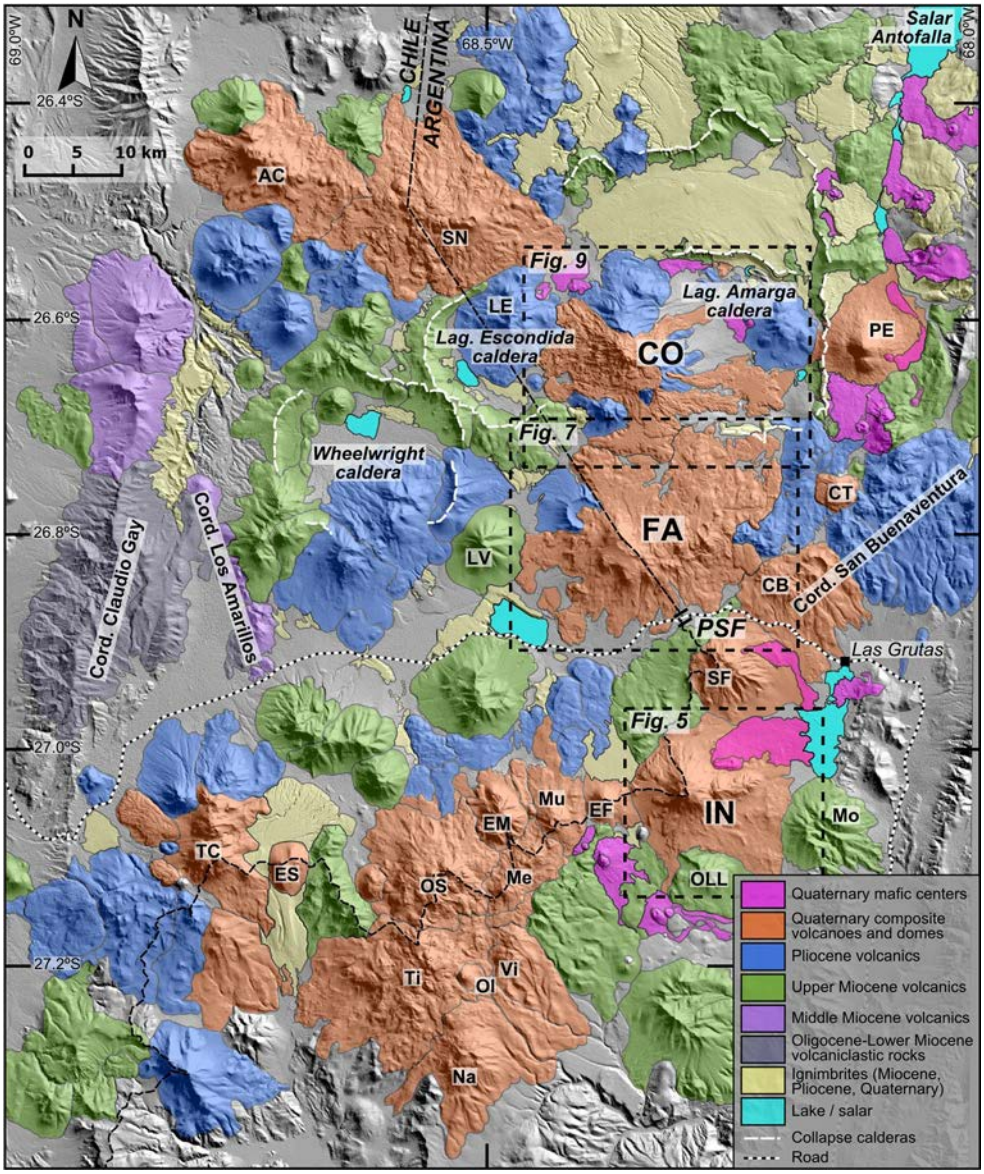

Fig. 2 Geological map of the Paso San Francisco (PSF) region of the Central Volcanic Zone of the Andes between 26.4° and 27.3° S latitude, from compilation of previous maps and references and our own work, draped on Shuttle Radar Topography Mission 30 m digital elevation model-derived shaded relief image. Volcanoes: CO: El Cóndor; FA: Falso Azufre; IN: Incahuasi; AC: Azufrera de Los Cuyanos; CB: Cerro Bertrand; CT: Cerro Torta; EF: El Fraile; EM: El Muerto; ES: El Solo; LE: Laguna Escondida; LV: Laguna Verde; Me: Medusa; Mo: Morocho; Mu: El Muertito; Na: Nacimientos; Ol: Olmedo; OLL: Ojo de Las Lozas; OS: Ojos del Salado; PE: Peinado; SF: San Francisco; SN: Sierra Nevada; TC: Tres Cruces; Ti: Tipas; Vi: del Viento

calderas (Wheelwright, Laguna Escondida and Laguna Amarga) and unknown sources were emplaced (e.g. González-Ferrán et al. 1985; Siebel et al. 2001; Schnurr et al. 2007; Clavero et al. 2012; Guzmán et al. 2014) (Fig. 2).

The Quaternary volcanic centers are built on top of the Upper Miocene and Pliocene centers (Fig. 2). Available K-Ar and Ar-Ar ages for the Quaternary centers span the Pleistocene up to 0.02 Ma (Table 1). Several centers form the ENE-WSW Ojos del Salado volcanic chain (González-Ferrán et al. 1985) (Fig. 2). These are, from west to east, the Tres Cruces massif, the El Solo dome, the Ojos del Salado massif, the El Muerto and El Muertito cones, the El Fraile dome and the Incahuasi cone. All these centers are dominantly dacitic, except for Incahuasi, which is dominantly andesitic (González-Ferrán et al. 1985; Baker et al. 1987; Mpodozis et al. 1996; Gardeweg et al. 2000). South and southeast of Ojos del Salado is the similar Tipas dacitic complex and other poorly known centers (Fig. 2). North of the Ojos del Salado chain are the San Francisco and Cerro Bertrand cones and the Falso Azufre massif, all of which are dominantly andesitic (Mpodozis et al. 1996; Kay et al. 2006; Clavero et al. 2012). Further north stands the El Cóndor massif, which lacks any previous studies, and the andesitic-dacitic Sierra Nevada-Azufrera de Los Cuyanos chain (Clavero et al. 2012; Polanco et al. 2014) (Fig. 2). At the eastern edge of the arc front, several mafic monogenetic centers, the mafic Peinado cone and the dacitic Cerro Torta lava dome are aligned NNE-SSW (Seggiaro et al. 2006) (Fig. 2).

Overall, the Quaternary volcanoes of the Paso San Francisco region follow the main N-S trend of the arc, but their vents and edifices show several different alignments (Fig. 2): WNW-ESE (Sierra Nevada-Azufrera de Los

Cuyanos), NNW-SSE (El Cóndor), NW-SE (western part of Falso Azufre), ENE-WSW (Ojos del Salado chain; eastern part of Falso Azufre), NNE-SSW (Peinado and several scoria cones) and N-S (Tres Cruces; volcanoes south of Ojos del Salado). These different trends may reflect the complex basement architecture of the southern CVZ, which contains sets of structures with different orientations that have been repeatedly reactivated and have localized magmatism (e.g. Chernicoff et al. 2002; Richards et al. 2006). North of the Paso San Francisco region, relationships between volcanism and the NW-SE trending Calama-Olacapato-El Toro and Archibarca lineaments (Fig. 1) have been well documented (e.g. Riller et al. 2001; Matteini et al. 2002; Richards and Villeneuve 2002; Petrinovic et al. 2006; Richards et al. 2006; Acocella et al. 2011; Norini et al. 2013). The Ojos del Salado lineament supposedly crosses the Paso San Francisco region (e.g. Salfity 1985), but there is no specific study on this lineament and its possible influence on the spatial distribution of volcanism is not clear.

In addition to composite volcanoes along the arc front, Quaternary mafic monogenetic centers are common, mainly in the backarc, especially in the Antofagasta de la Sierra region (Fig. 1), with a peak of activity at < 1 Ma (Risse et al. 2008). Moreover, three collapse caldera centers formed during the Quaternary, with associated ignimbrites and domes: Cerro Galán, with its main collapse at 2.08 Ma (e.g. Sparks et al. 1985; Folkes et al. 2011; Kay et al. 2011), Cerro Blanco, 0.44 to < 0.005 Ma (e.g. Kraemer et al. 1999; Seggiaro et al. 2006; Montero López et al. 2010; Báez et al. 2015) and Incapillo, 0.51 Ma (Goss et al. 2009), at the southern termination of the CVZ (Fig. 1).

Methods

Mapping and volcano morphometry

Mapping of volcanic units was performed on a GIS platform (QGIS Geographic Information System: http://qgis.osgeo.org) and was based on fieldwork, the interpretation of Landsat 7 ETM and GoogleEarth satellite images and the Shuttle Radar Topography Mission (SRTM) 30 m digital elevation model (DEM), as well as published geological maps (Mpodozis et al. 1996; Gardeweg et al. 1997; Seggiaro et al. 2006; Clavero et al. 2012).

Morphometric data for the studied volcanoes were obtained applying the MORVOLC algorithm (Grosse et al. 2009, 2012; http://cediac.uncu.edu.ar/software/) on the SRTM 30 m DEM. Acquired morphometric parameters include the areal extents, widths, heights and volumes of edifices and main units. The mapped outlines of edifices and units were used to compute exposed areas and widths. For the estimation of heights and volumes, MORVOLC fits an inverse distance weighting (IDW) basal surface to the outlines; height is the maximum vertical distance between this basal surface and the DEM surface, and volume is the integrated sum of the space between both surfaces. Further measurements of smaller features such as individual lava flows (lengths, widths, thicknesses) and craters (diameters) were obtained directly with the GIS software. The Quaternary volcanoes of the Paso San Francisco region were classified into morphometric types (Table 1) following Grosse et al. (2009, 2017).

Sampling, petrography and whole-rock geochemistry

A total of 55 samples were collected from the Incahuasi, Falso Azufre and El Cóndor volcanoes during fieldwork. Petrographic analyses of 44 thin sections aided in the correlation of units (petrographic results are not presented as they are beyond the scope of this contribution). Twenty-six representative and unaltered samples were chosen for whole-rock chemical analyses, performed at the Earthquake Research Institute, University of Tokyo (Japan). Major elements were determined by the X-ray fluorescence (XRF) method (Rigaku ZSX Purimas II). The error is estimated to be 5% based on reproducibility of repeat measurements of the rock standard JB-1b issued by the Geological Survey of Japan. Rocks were classified using the total alkalis silica (TAS) diagram (Le Maitre et al. 1989) (Fig. 3) and the K_2O vs. SiO_2 diagram (Peccerillo and Taylor 1976) (not shown), on a volatile-free basis. Major element geochemistry of representative samples is presented in Table 2.

K-Ar geochronology

The same 26 samples that were geochemically analyzed were dated by the unspiked K-Ar method on whole-rock samples. In this technique, the radiogenic ^{40}Ar concentration is determined by a direct comparison of the $^{40}Ar/^{36}Ar$ ratio and the ^{40}Ar signal intensity of the samples with those of a volumetrically calibrated amount of atmospheric Ar at the same condition of the mass spectrometer. The technique can precisely date rocks younger than 0.1 Ma (as demonstrated by recent studies, e.g. Guillou et al. 2010; Samaniego et al. 2016) since it allows measurement of small amounts of radiogenic Ar and determines the isotopic composition of the initial Ar in the sample by measuring $^{38}Ar/^{36}Ar$ without assuming that the $^{40}Ar/^{36}Ar$ ratio in the sample is equal to the modern atmospheric value of 296 (e.g. Gillot et al. 1982; Nagao et al. 1991; Matsumoto and Kobayashi 1995; Orihashi et al. 2004; Scaillet and Guillou 2004).

Samples were crushed by a jaw crusher and sieved to 60–80 mesh size. The ferromagnetic minerals were separated using a hand magnet. Samples were then washed in an ultrasonic bath. The same material was used for both K and Ar

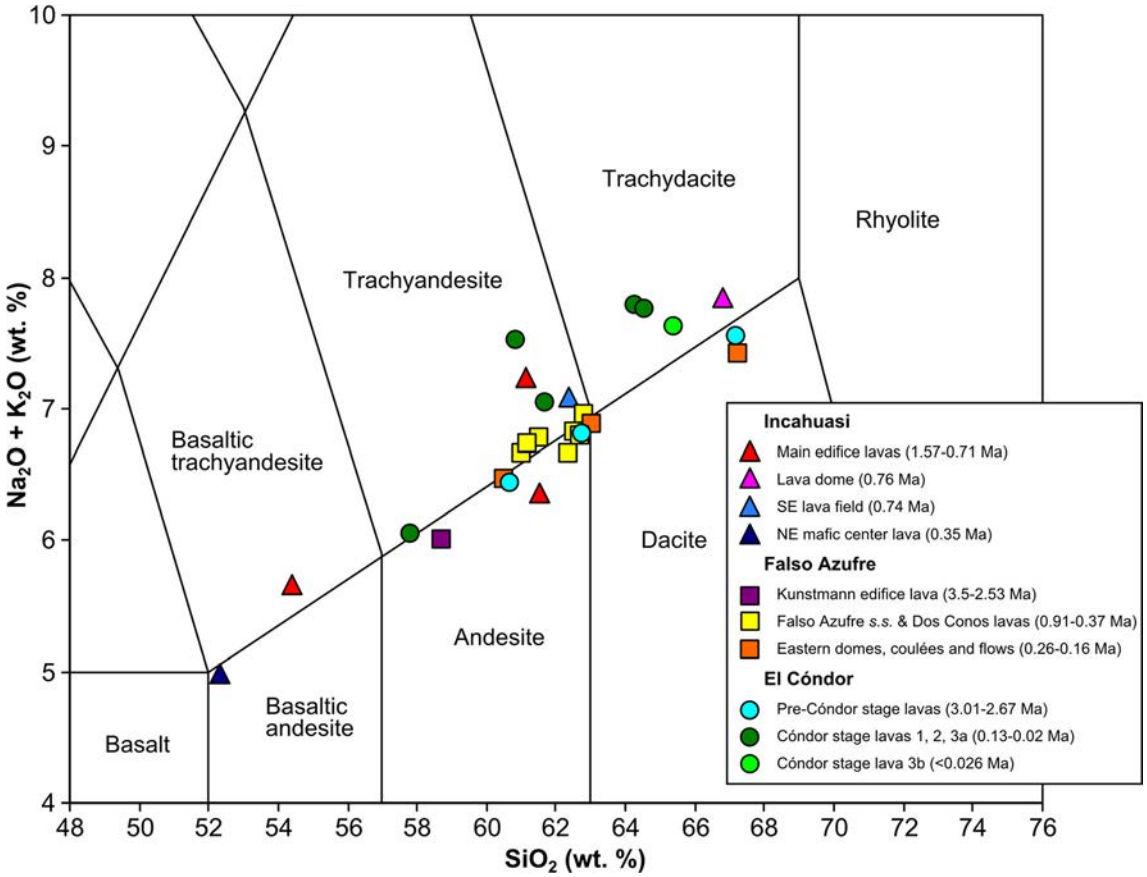

Fig. 3 Classification of rocks from the Incahuasi, Falso Azufre and El Cóndor volcanoes in the total alkalis silica (TAS) diagram of Le Maitre et al. (1989)

analyses. Ar isotopes were analyzed using a noble gas mass spectrometer MS-III (modified-VG5400) at the Geochemical Research Center, University of Tokyo. The sensitivity of the mass spectrometer for ^{40}Ar and mass discrimination factors for $^{38}Ar/^{36}Ar$ and $^{40}Ar/^{36}Ar$ ratios were determined with measurements of atmospheric Ar standard (1.5×10^{-7} cm^3 STP). The error on ^{40}Ar sensitivity is estimated to be 5% based on reproducibility of the repeated measurements of the standard. The errors on $^{38}Ar/^{36}Ar$ and $^{40}Ar/^{36}Ar$ ratios, which were maintained below 0.2%, include statistical errors during signal acquisition of the measurements of samples and that of the standard. K concentration was determined by the XRF method at the Earthquake Research Institute, University of Tokyo. Further details on the method, including the error calculation on the age determinations, can be found in Nagao et al. (1991, 1996) and Orihashi et al. (2004).

The geochronological results are shown in Table 3 and Fig. 4. Thirteen samples have $^{38}Ar/^{36}Ar$ ratios in agreement with the modern atmospheric value of 0.1880, within the range of analytical error (1σ). The other samples have $^{38}Ar/^{36}Ar$ ratios either lower (five samples) or higher (eight samples) than the atmospheric value beyond the range of the analytical error. In these cases, the mass fractionation effect was corrected by using the measured $^{38}Ar/^{36}Ar$ ratios of the samples, and then K-Ar ages were recalculated; the resulting analytical errors are larger for these samples due to the insufficient accuracy of the measured $^{38}Ar/^{36}Ar$ ratio for the correction of mass fractionation.

Estimation of volumes, lifespans and growth rates

DEM-derived volumes suffer from a number of uncertainties that can be linked to the properties of the DEM (accuracy, resolution), the delineation of the unit outlines, the interpolation methods used and, more significantly, the coalescence of units and the assumption of a uniformly sloping original topography beneath the volcano or unit. For coalescing units, obtained heights and volumes are realistic values for the younger units, but are too low for the older units or for units of equal age. For the later, better estimates were obtained considering an IDW basal surface fitted only to the outline elevations that do not coalesce. For the older units, assuming that they have a continuation below the younger units, an excess volume was estimated adding the volume of a wedge located below the younger unit.

To take into account these uncertainties, we have added to each volume estimate (V) a somewhat arbitrary uncertainty value (σ_V) considering uncertainties of ± 10 to ± 100 m over

Table 2 Whole-rock major element geochemistry (wt.%) of representative samples of Incahuasi, Falso Azufre and El Cóndor volcanoes

	Incahuasi					Falso Azufre						El Cóndor					
Unit	Main edifice		Lava dome	SE lava field	NE mafic center	Kunstmann edifice	Falso Azufre s.s. edifice		Dos Conos edifice		Eastern domes, coulées and flows		Pre-Cóndor stage		Cóndor stage			
Sample	IN01	IN11	IN07	IN16	IN09	FA13	FA08	FA12	FA02	FA04	FA01	FA07	CO08	CO15	CO03	CO07	CO01	CO06
SiO_2	60.8	54.3	66.3	61.6	52.0	58.2	60.6	61.6	62.4	61.9	66.8	62.7	62.2	60.3	57.3	63.8	60.9	65.2
TiO_2	0.78	0.99	0.54	0.80	1.22	0.83	0.82	0.78	0.78	0.80	0.58	0.67	0.75	0.79	0.96	0.65	0.86	0.69
Al_2O_3	16.37	17.35	15.19	16.49	14.52	16.85	16.47	15.78	16.05	16.86	15.13	15.73	16.67	15.92	16.63	17.09	17.41	15.83
$Fe_2O_3^T$	5.98	8.17	3.78	5.19	8.50	6.95	5.87	5.76	5.27	5.82	3.74	5.06	5.34	5.96	7.09	3.98	5.53	4.36
MgO	2.87	5.13	1.86	2.46	9.53	3.81	3.01	3.03	2.59	2.60	1.74	3.22	2.15	4.00	4.07	1.50	2.40	1.81
MnO	0.09	0.13	0.07	0.08	0.14	0.11	0.09	0.09	0.08	0.09	0.07	0.08	0.09	0.10	0.11	0.08	0.08	0.07
CaO	5.42	7.81	3.52	4.92	8.20	6.15	5.56	4.94	4.83	5.30	3.57	5.02	4.99	5.71	6.70	4.22	5.07	3.92
Na_2O	3.44	3.67	3.68	3.77	3.02	3.52	3.84	3.44	3.86	3.76	3.56	3.53	3.39	3.38	3.48	4.25	4.09	3.62
K_2O	2.85	1.99	4.12	3.23	1.91	2.44	2.76	3.13	3.05	3.07	3.80	3.32	3.36	3.02	2.52	3.49	3.44	3.97
P_2O_5	0.19	0.28	0.21	0.22	0.36	0.25	0.24	0.20	0.24	0.23	0.17	0.18	0.24	0.20	0.25	0.23	0.29	0.19
Total	98.76	99.78	99.26	98.74	99.36	99.12	99.22	98.71	99.38	100.64	99.36	99.55	99.20	99.33	99.09	99.28	100.04	99.63
Composition[a]	A	BTA	TD	TA	BA	A	TA	A	TA	TA	D	A	A	A	TA	TD	TA	TD

BA basaltic andesite, *BTA* basaltic trachyandesite, *A* andesite, *TA* trachyandesite, *D* dacite, *TD* trachydacite

[a] Classification using the total alkalis silica (TAS) diagram (Le Maitre et al. 1989)

Table 3 Unspiked K-Ar ages for samples of Incahuasi, Falso Azufre and El Cóndor volcanoes

Sample	Unit	Composition[a]	Location		K	^{40}Ar rad	^{38}Ar/36Ar	(^{40}Ar/^{36}Ar)initial[b]	Age	Air Fraction
			Lat. (°)	Lon. (°)	(wt.%)	10^{-8} cm^{3}STP/g		Fractionated Ar assumed	(Ma)	(%)
Incahuasi										
IN01	Main edifice	A	−26.9928	−68.2878	2.44 ± 0.12	7.87 ± 0.43	0.1896 ± 0.0016		1.569 ± 0.099	58.68
IN11	Main edifice	BTA	−27.0747	−68.2769	1.618 ± 0.081	6.28 ± 0.77	0.18615 ± 0.00086	290.2 ± 2.7	1.00 ± 0.13	90.80
IN13	Main edifice	TA	−27.0724	−68.2500	2.49 ± 0.12	11.0 ± 3.6	0.1891 ± 0.0010	299.4 ± 3.2	1.14 ± 0.37	96.42
IN07	Lava dome	TD	−27.0210	−68.2155	3.31 ± 0.17	9.8 ± 1.1	0.18792 ± 0.00086		0.763 ± 0.085	95.41
IN16	SE lava field	TA	−27.0445	−68.1861	2.87 ± 0.14	8.23 ± 0.48	0.19050 ± 0.00070	303.9 ± 2.2	0.739 ± 0.048	66.33
IN09	NE mafic center	BA	−27.0073	−68.1704	1.291 ± 0.065	1.77 ± 0.16	0.1906 ± 0.0010	304.3 ± 3.3	0.352 ± 0.033	85.93
Falso Azufre										
FA13	Kunstmann edifice	A	−26.7705	−68.4476	2.01 ± 0.10	19.7 ± 1.8	0.18700 ± 0.00096	301.4 ± 3.0	2.525 ± 0.243	84.75
FA08	Falso Azufre s.s. edifice	TA	−26.8755	−68.4285	2.24 ± 0.11	5.61 ± 0.51	0.19009 ± 0.00056	302.6 ± 0.5	0.644 ± 0.062	91.44
FA12	Falso Azufre s.s. edifice	A	−26.7231	−68.4097	2.25 ± 0.11	4.61 ± 0.80	0.18792 ± 0.00059		0.528 ± 0.093	97.02
FA14	Falso Azufre s.s. edifice	A	−26.7960	−68.4432	2.32 ± 0.12	5.96 ± 0.56	0.18815 ± 0.00086		0.662 ± 0.065	93.78
FA15	Falso Azufre s.s. edifice	TA	−26.8802	−68.3385	2.30 ± 0.11	5.7 ± 1.9	0.1877 ± 0.0011		0.64 ± 0.22	97.87
FA02	Dos Conos edifice (summit region)	TA	−26.8185	−68.3059	2.31 ± 0.12	3.34 ± 0.29	0.1901 ± 0.0018	302.7 ± 5.7	0.373 ± 0.035	74.62
FA04	Dos Conos edifice	TA	−26.8550	−68.2851	2.30 ± 0.12	8.2 ± 2.0	0.18820 ± 0.00077		0.91 ± 0.22	97.02
FA17	Dos Conos edifice	A	−26.7239	−68.2099	2.42 ± 0.12	6.7 ± 1.8	0.18689 ± 0.00076	292.5 ± 2.4	0.71 ± 0.19	96.45
FA01	Eastern domes, coulées and flows	D	−26.8268	−68.2212	3.15 ± 0.16	3.2 ± 3.8	0.18740 ± 0.00049	294.1 ± 1.5	0.26 ± 0.31	99.46
FA06	Eastern domes, coulées and flows	A	−26.8396	−68.2521	2.16 ± 0.11	2.17 ± 0.68	0.18846 ± 0.00074		0.259 ± 0.081	98.42
FA07	Eastern domes, coulées and flows	A	−26.7335	−68.1996	2.31 ± 0.12	1.43 ± 0.75	0.1882 ± 0.0015		0.160 ± 0.083	99.29
El Cóndor										
CO08	Pre-Cóndor stage (Condorito)	A	−26.7033	−68.3997	2.83 ± 0.14	30.2 ± 1.3	0.18999 ± 0.00079	302.3 ± 2.5	3.01 ± 0.15	53.19
CO14	Pre-Cóndor stage	D	−26.5404	−68.3481	3.07 ± 0.15	34.53 ± 2.18	0.18806 ± 0.00063		2.89 ± 0.20	89.19
CO15	Pre-Cóndor stage	A	−26.5367	−68.3770	2.37 ± 0.12	25.0 ± 1.4	0.18846 ± 0.00098		2.67 ± 0.19	74.12
CO03	Cóndor stage (lavas 1)	TA	−26.6448	−68.1879	2.00 ± 0.10	2.18 ± 0.36	0.18542 ± 0.00065	287.9 ± 2.1	0.128 ± 0.023	97.76
CO07	Cóndor stage (lavas 2)	TD	−26.7092	−68.3982	2.80 ± 0.14	1.0 ± 1.7	0.1877 ± 0.0010		0.09 ± 0.15	99.69
CO01	Cóndor stage (lavas 3a)	TA	−26.6832	−68.2438	2.85 ± 0.14	0.40 ± 0.14	0.19048 ± 0.00081	303.8 ± 2.6	0.036 ± 0.012	97.03
CO11	Cóndor stage (lavas 3a)	TA	−26.6404	−68.2655	2.91 ± 0.15	< 0.85	0.1878 ± 0.0010		< 0.075	100.3
CO22	Cóndor stage (lavas 3a)	TD	−26.6414	−68.4533	3.34 ± 0.17	0.30 ± 0.33	0.18918 ± 0.00088	299.7 ± 2.8	0.023 ± 0.025	99.06
CO06	Cóndor stage (lavas 3b)	TD	−26.5983	−68.3121	3.20 ± 0.16	< 0.32	0.1881 ± 0.0011		< 0.026	100.2

BA basaltic andesite, *BTA* basaltic trachyandesite, *A* andesite, *TA* trachyandesite, *D* dacite, *TD* trachydacite

[a] Classification using the total alkalis silica (TAS) diagram (Le Maitre et al. 1989)

[b] (^{40}Ar/^{36}Ar)initial = 296.0 is assumed. Error: 1σ

(^{40}Ar/^{36}Ar)initial was estimated from the measured ^{38}Ar/^{36}Ar ratio, which was fractionated from the atmospheric value of 0.1880

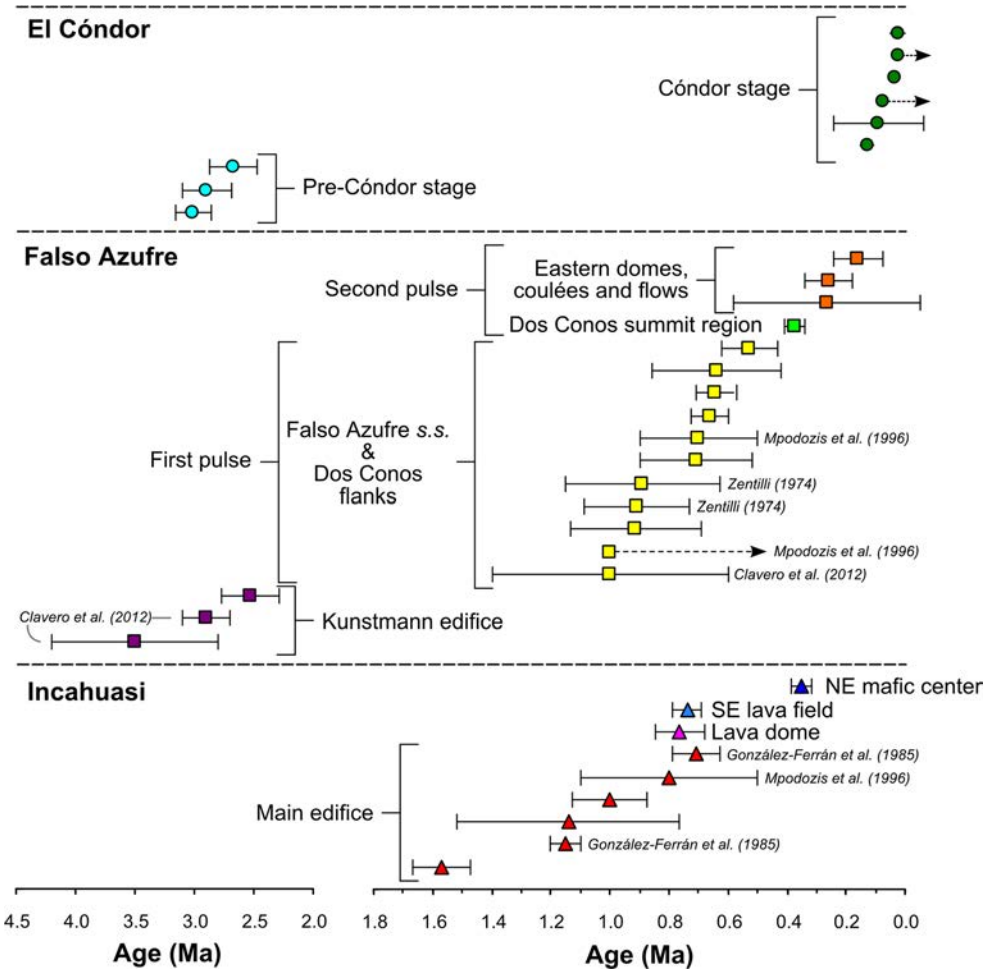

Fig. 4 Available absolute ages (with 1σ uncertainty error bars) for the three studied volcanoes; ages without references are from this study

the area of the underlying basal surface, depending on how well-defined the unit is, the inferred roughness of the underlying topography and its size. This results in uncertainties mostly between 10 and 20% (and up to 60%) of the total values, similar or larger than those considered in equivalent studies (e.g. Frey et al. 2004; Hora et al. 2007). Note that these uncertainties will spread to the estimated growth rates (see below). Two further sources of uncertainty come from the volumes lost through erosion and ash dispersal due to explosive volcanism. However, for the studied volcanoes, these uncertainties can be considered negligible compared to the above-mentioned uncertainties, taking into account the arid climate, the fresh appearance of the deposits, the lack of evidence of glacial erosion and the mostly effusive character of the volcanoes. The calculated volumes are bulk volumes.

Lifespans (L) were estimated as the time interval between the oldest (Age_{MAX}) and youngest (Age_{MIN}) ages available for each volcano or unit. Lifespan uncertainties (σ_L) were estimated considering the 1 sigma errors (1σ) of these ages:

$$\sigma_L = (L_{MAX} - L_{MIN})/2$$

where $L_{MAX} = (Age_{MAX} + 1\sigma) - (Age_{MIN} - 1\sigma)$ and $L_{MIN} = (Age_{MAX} - 1\sigma) - (Age_{MIN} + 1\sigma)$.

Volumes and lifespans allow calculating overall growth rates, $GR = V / L$, with a growth rate uncertainty range (σ_{GR}) given by maximum (GR_{MAX}) and minimum (GR_{MIN}) possible growth rates:

$$GR_{MAX} = (V + \sigma_V)/(L - \sigma_L)$$

$$GR_{MIN} = (V - \sigma_V)/(L + \sigma_L)$$

Results

Incahuasi volcano

At over 6600 m elevation, Incahuasi is one of the highest volcanoes on Earth. It straddles the Argentina-Chile border, occupying an area of 207 km^2 (Fig. 5). Incahuasi is the easternmost volcano of the Ojos del Salado chain and is bounded to the north by the Quaternary San Francisco volcano and by Upper Miocene volcanic rocks, and to the south and southeast

by the Upper Miocene Cerro Ojo de Las Lozas and Cerro Morocho volcanoes (Figs. 2 and 5).

Incahuasi consists of a main steep-sided conical edifice and three peripheral units located on its eastern flanks (Figs. 5 and 6): a large lava dome, a small lava field and a mafic monogenetic center. The main edifice is 13 km wide at the base and 1.9 km high. It has a relatively flat 2 km-wide summit region capped by a summit crater (900 × 750 m). The main edifice flanks consist of moderately preserved blocky lava flows < 1 km wide and < 5 km long (Flank lava flows; Figs. 5 and 6); the best-preserved flows on the southern flank show levees and flow ridges. In the summit region, two thick, stubby coulées with well-preserved ridges flow north and east of the crater (Summit region coulées; Figs. 5 and 6).

The steep-sided lava dome on the eastern flank of the main edifice gives the volcano an overall ENE-WSW elongation (Lava dome; Figs. 5 and 6). It has a 6 × 4 km base and is 0.6 km high. Southeast of the lava dome and on the lower ESE flank of the main edifice is a 18 km^2 field of dark lava flows whose vents are not clearly identified (SE lava field; Fig. 5). On the NE flank of the main edifice, a set of pristine overlapping scoria cones produced extensive dark, well-preserved blocky and ‘a‘ā lava flows that spread towards the NE and E, covering 41 km^2 and extending up to ca. 8 km from the vents (NE mafic center; Figs. 5 and 6). This center is part of a group of mafic centers aligned SSW-NNE from south of Incahuasi to the southern tip of the Antofalla salar (Grosse et al. 2014b; Ochi Ramacciotti et al. 2017) (Fig. 2).

The main edifice flank lava flows range from basaltic trachyandesites to andesites and trachyandesites, whereas the lava dome is trachydacitic (Fig. 3; Table 2). Lava flows of the NE mafic center are basaltic andesites, and one lava flow sample of the SE lava field is trachyandesitic (Fig. 3; Table 2). All samples belong to the high-K calc-alkaline series.

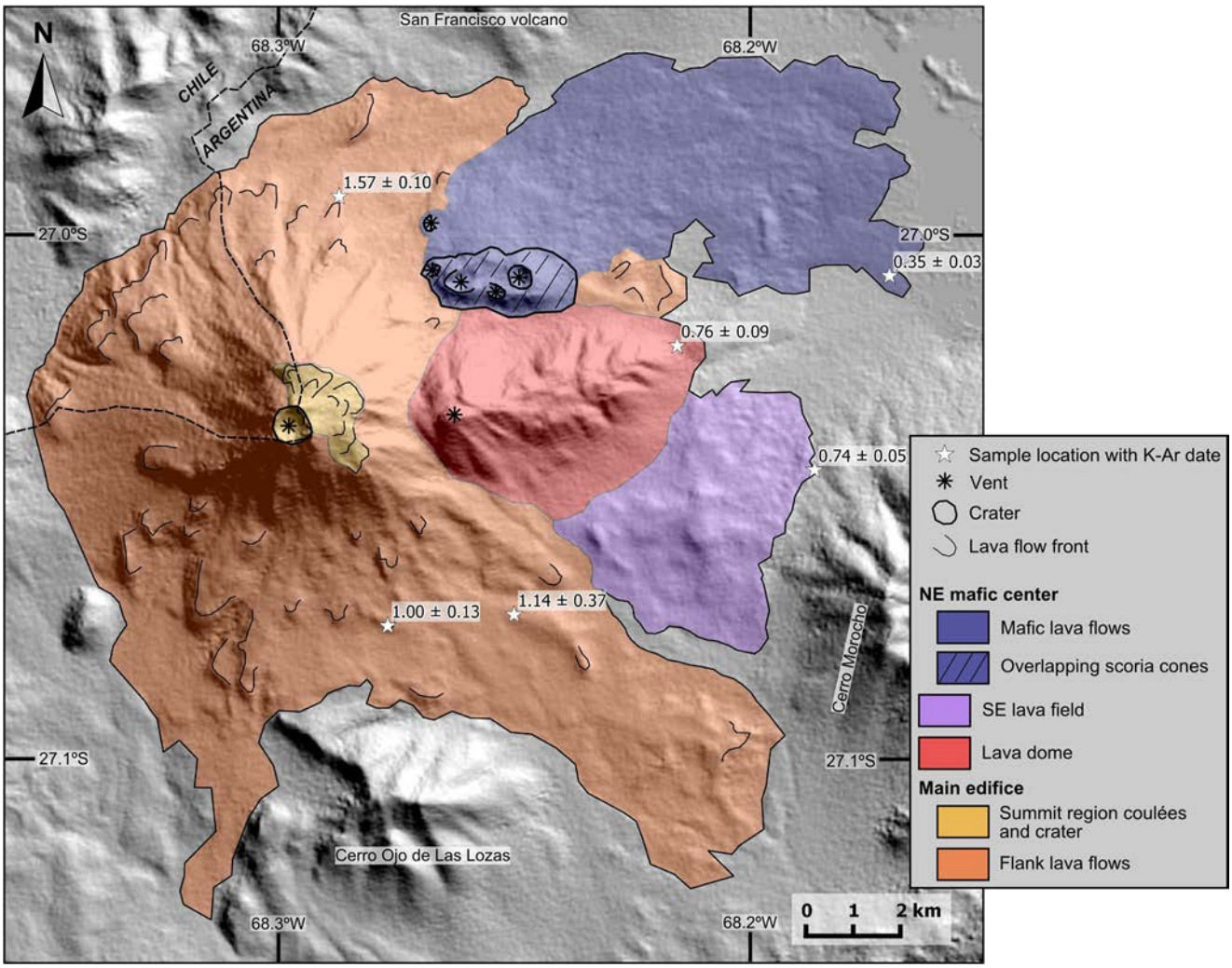

Fig. 5 SRTM 30 m DEM-derived shaded relief image of Incahuasi volcano showing volcanic units and features and new K-Ar ages

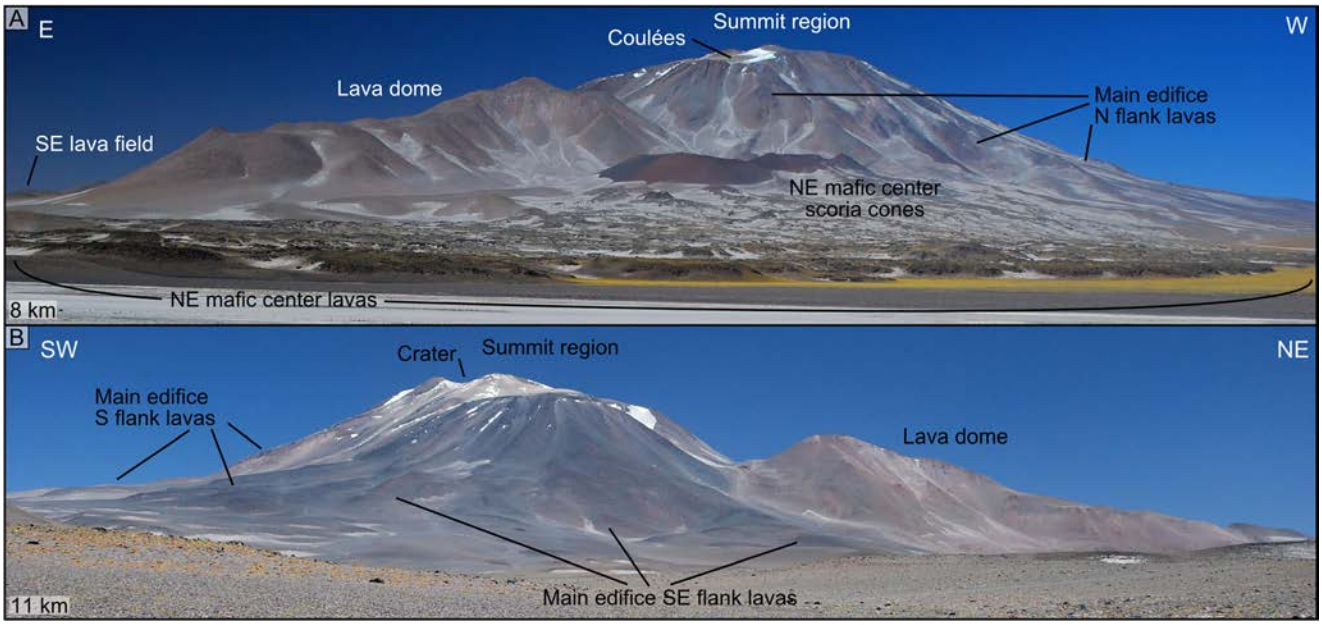

Fig. 6 Panoramic views of Incahuasi volcano from **a** Northeast and **b** Southeast. Values at the lower left of each photograph are the approximate horizontal distances covered by the images

K-Ar ages

Two lava flows from the NW and N flanks of the main edifice have been previously dated by the conventional K-Ar method. González-Ferrán et al. (1985) obtained ages of 0.71 ± 0.08 Ma on whole-rock and 1.15 ± 0.05 Ma on biotite crystals, whereas Mpodozis et al. (1996) obtained an age of 0.80 ± 0.30 Ma on whole-rock.

We have obtained six new K-Ar ages (Table 3; Figs. 4 and 5). Three ages are of lava flows from the main edifice flanks. The least well-preserved dated lava belongs to a small andesitic flow on the northern flank that yielded an age of 1.57 ± 0.10 Ma. A sample from a thick trachyandesitic flow on the SE flank gave an age of 1.14 ± 0.37 Ma, and a thin basaltic trachyandesite flow on the SSE flank yielded an age of 1.00 ± 0.13 Ma. The lava dome (0.76 ± 0.09 Ma) and the SE lava field (0.74 ± 0.05 Ma) have similar ages within error. The youngest recorded age of 0.35 ± 0.03 Ma is of a lava flow from the NE mafic center.

Falso Azufre volcano

Falso Azufre is an elongated massif straddling Argentina and Chile, reaching an elevation of ca. 5900 m. It has numerous vents that are aligned in two main directions, NW-SE on the western side and ENE-WSW on the eastern side, conferring an arcuate plan shape to the whole massif (Fig. 7). It is one of the largest massifs of the region, covering an area of 387 km^2, with approximate basal diameters of 25 × 20 km and a height of 1.2 km. It is constructed mainly by numerous (ca. 50 exposed) blocky lava flows covering all flanks (Fig. 7), some of which are very voluminous, up to 7 km long and 4 km wide.

Falso Azufre stands northwest of the San Francisco volcano and south of the Laguna Amarga caldera (Figs. 2, 7 and 8). It is bounded to the east by Pliocene volcanic rocks and to the west by the Upper Miocene Laguna Verde volcano and Miocene/Pliocene volcanic rocks (Figs. 2 and 7). To the north, its lava flows are in contact with flows from El Cóndor volcano (Figs. 2 and 7).

The NW side of Falso Azufre is formed by the morphologically oldest part of the massif, the Kunstmann edifice (González-Ferrán et al. 1985; Clavero et al. 2012; Figs. 7 and 8). This edifice has smooth flanks and is truncated by a 3-km-wide collapse scar open towards the SE and filled by younger lavas (Fig. 7). On the lower SW flank of the massif, there is a small, 2-km-wide edifice with short stubby lava flows (SW edifice; Figs. 7 and 8) that appears to be older than the main edifice of Falso Azufre, as it has diverted its lava flows.

The highest and main edifice of the complex (Falso Azufre sensu stricto) occupies the central-western part of the massif (Figs. 7 and 8). It has a relatively large and flat summit region occupied by a main crater (1.3 × 1 km) on the NW end, and several minor craters and vents (with diameters ranging between 0.3 and 0.6 km) aligned towards the SE (Falso Azufre *s.s.* summit region; Fig. 7). We interpret from satellite image analysis that this summit region is blanketed by pyroclastic deposits, as was previously suggested by de Silva and Francis (1991). The flanks of the main edifice are covered by several lava flows extending towards the N, W and S (Falso Azufre *s.s.* flank lava flows; Figs. 7 and 8).

The eastern part of the massif is made up of the Dos Conos edifice (Figs. 7 and 8). Its summit region, bounded to the south by a ENE-WSW-oriented scarp, consists of two small, steep cones, other minor eruptive vents and several short lava flows (Dos Conos summit region; Figs. 7 and 8). Both voluminous and small lava flows cover the N and S flanks of the edifice (Dos Conos flank lava flows; Figs. 7 and 8).

At the eastern edge of the massif, two large coulées (3 and 5 km long), a large dome and its associated lava flow (7 km long), small stubby flows and five small (diameters of ~ 400 m) domes lay on top of the Dos Conos flank lavas or intrude older volcanic rocks (Eastern domes, coulées and flows; Figs. 7 and 8). Their pristine morphology suggests that this unit is the youngest of the massif. The Dos Conos edifice and the Eastern unit are cut by several lineaments and faults striking ENE-WSW to E-W (Fig. 7).

A sample of the Kunstmann edifice is andesitic and has the lowest SiO_2 concentration (58%), whereas all other lavas of the massif have $SiO_2 > 60\%$. The lava flows of the Falso Azufre *s.s.* and Dos Conos edifices are andesitic or trachyandesitic. The Eastern unit domes and coulées are dacitic, whereas the Eastern unit flows are andesitic, similar to the andesites of the main edifices (Fig. 3; Table 2). All samples of Falso Azufre belong to the high-K calc-alkaline series. At several locations, the massif has undergone strong hydrothermal alteration (Figs. 7 and 8).

K-Ar ages

There are seven previous K-Ar ages of lavas from Falso Azufre. Zentilli (1974) obtained ages of 0.91 ± 0.18 and 0.89 ± 0.26 Ma for andesitic lavas on the southern flank. Mpodozis et al. (1996) obtained ages of 0.70 ± 0.20 Ma for an andesite flow on the western flank and < 1 Ma for an andesite on the southeastern flank. Clavero et al. (2012) obtained an age of 1.0 ± 0.4 Ma for a dacite on the NW flank and two ages of 2.9 ± 0.2 and 3.5 ± 0.7 Ma for andesites belonging to the Kunstmann edifice.

We have obtained 11 new K-Ar ages (Table 3; Figs. 4 and 7). The oldest age of 2.53 ± 0.24 Ma is of a lava flow from the Kunstmann edifice; all other ages are < 1 Ma. Six samples of the Falso Azufre *s.s.* and of the Dos Conos flank lava flows have ages between 0.9 and 0.5 Ma. They belong to lavas located on the S (0.64 ± 0.22 Ma), SW (0.64 ± 0.06 Ma), W (0.66 ± 0.07 Ma) and N (0.53 ± 0.09 Ma) flanks of the Falso Azufre *s.s.* edifice, and on the S (0.91 ± 0.22 Ma) and NE (0.71 ± 0.19 Ma) flanks of the Dos Conos edifice (Fig. 7).

The remaining four samples have ages < 0.4 Ma and belong to the Dos Conos summit region and the Eastern unit. A

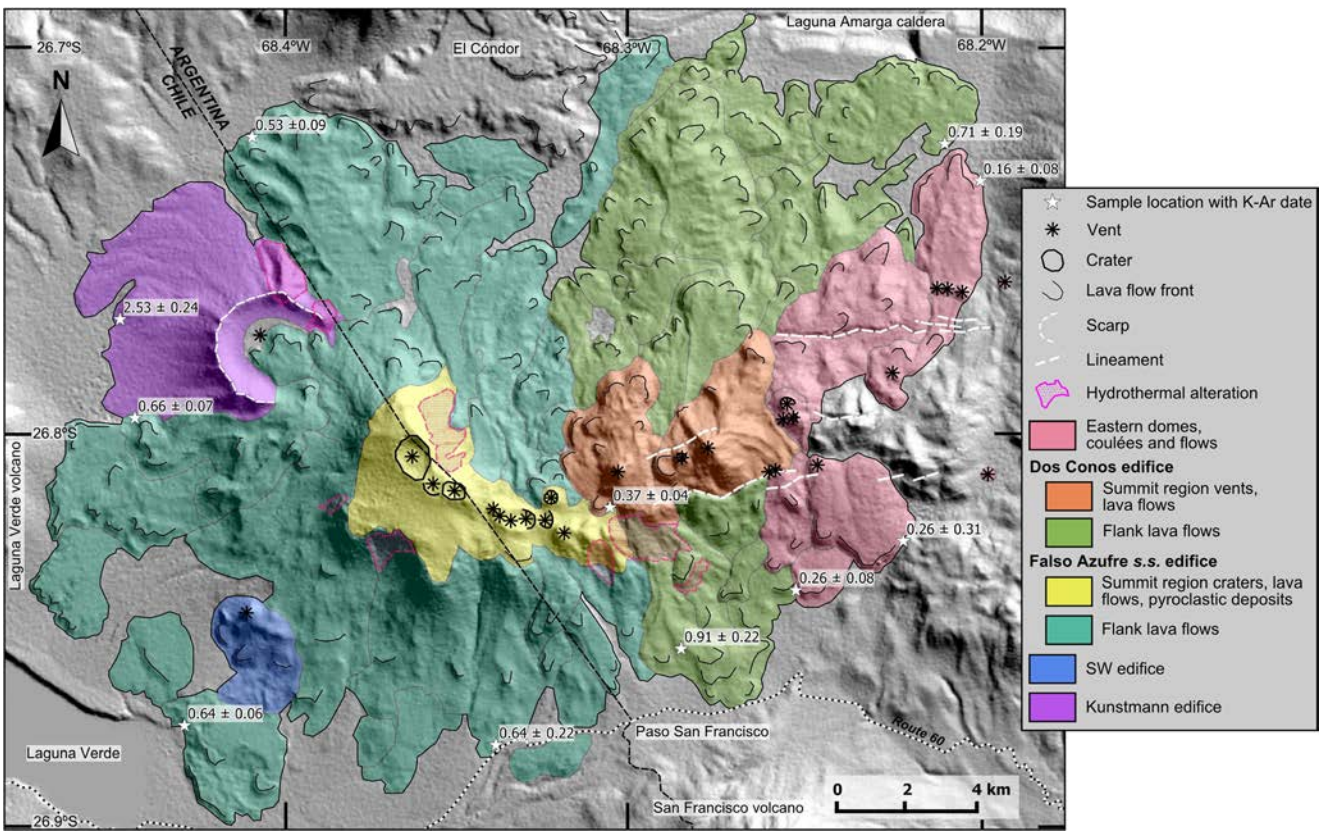

Fig. 7 SRTM 30 m DEM-derived shaded relief image of Falso Azufre volcano showing volcanic units and features and new K-Ar ages

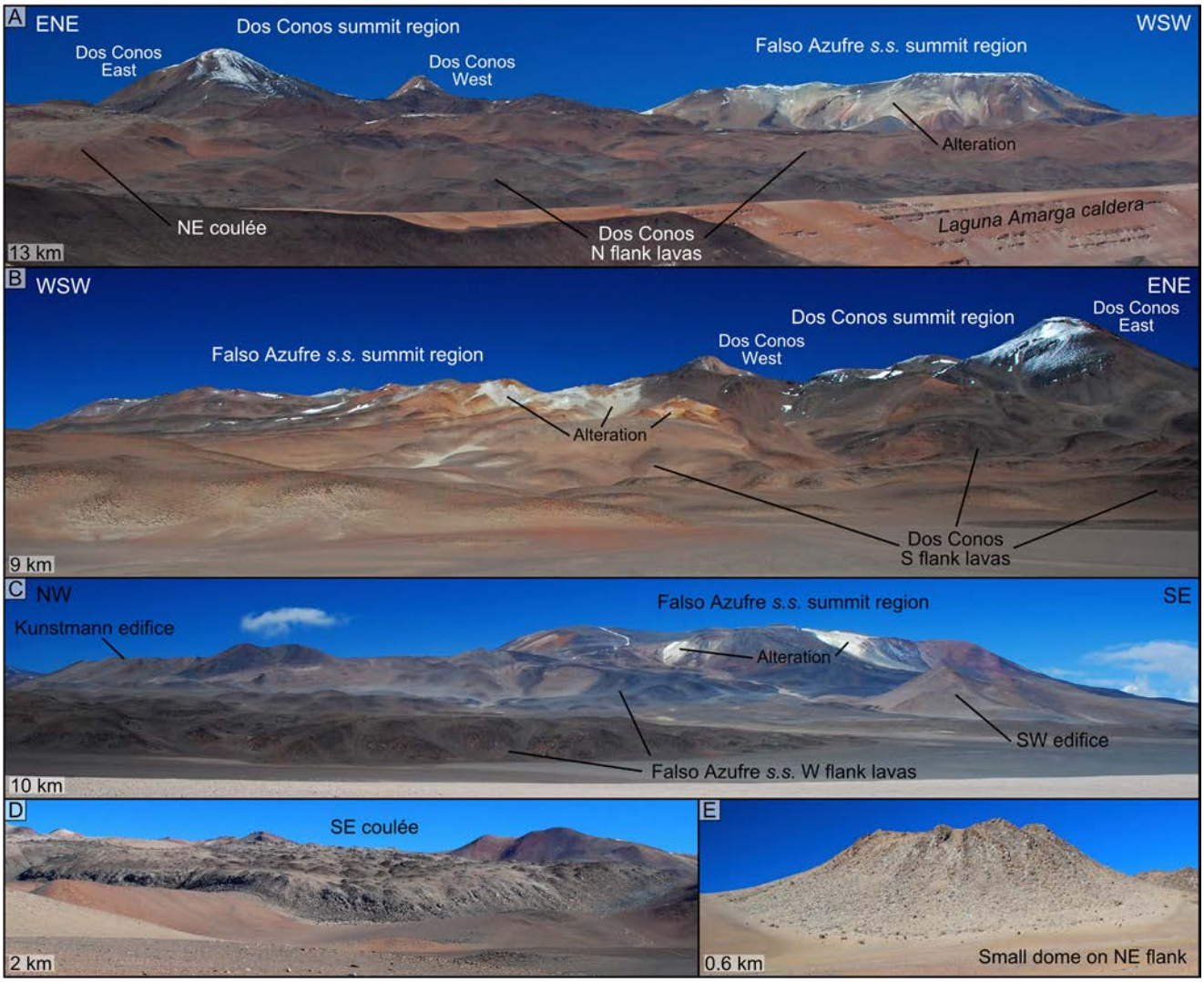

Fig. 8 Panoramic views of Falso Azufre volcano from **a** Northeast, **b** Southeast and **c** Southwest; **d** large coulée on SE flank; **e** small dome on NE flank. Values at the lower left of each photograph are the approximate horizontal distances covered by the images

short lava flow in the Dos Conos summit region, at the SW foot of the western cone, gave an age of 0.37 ± 0.04 Ma (Fig. 7). A small thick flow on the SE flank of the massif has an age of 0.26 ± 0.08 Ma (Fig. 7). The large southeastern dacitic coulée gave an uncertain age with a large error (0.26 ± 0.31 Ma); however, its stratigraphic position on top of the flow with an age of 0.26 ± 0.08 Ma indicates it is younger than this age (hence, its age can be adjusted to < 0.34 Ma). The youngest obtained age of 0.16 ± 0.08 Ma belongs to the lava flow of the eastern dome and associated flow (Fig. 7).

El Cóndor volcano

El Cóndor volcano is located in an extremely remote region, entirely within Argentina, reaching an elevation of ca. 6400 m. It covers the western part of the Laguna Amarga caldera (Figs. 2 and 9). The distribution of its lava flows was constrained by the Laguna Escondida volcano to the NW, an unnamed volcano to the SW (we name it Condorito) and by Falso Azufre lavas to the S (Figs. 2 and 9). To the N, the volcano covers the Lower Pliocene Laguna Amarga Ignimbrite, whereas to the east, El Cóndor lavas were free to flow long distances across the floor of the Laguna Amarga caldera (Figs. 2, 9 and 10).

El Cóndor is a NNW-SSE elongated massif and covers an area of 281 km^2; its height is estimated at 1.8 km. Two distinct stages of activity are evident, an older pre-Cóndor stage, and a more recent Cóndor stage (Fig. 9).

The pre-Cóndor units make up most of the northern flank of the massif and parts of the eastern and southeastern flanks (Main pre-Cóndor edifice; Figs. 9 and 10). The upper parts of these flanks show large scarps. The 2.5-km-wide SE scarp open towards the west, looks very much like a caldera remnant. The lower flanks of the northern pre-Cóndor sector consist of a few relatively well-preserved lava flows and two

possible domes. To the SW, El Cóndor volcano abuts with the small Condorito edifice which can be considered also part of the pre-Cóndor stage (Condorito edifice; Figs. 9 and 10). It is a 0.7-km-high conical edifice with a 4 km base and truncated by a large 1.4-km-wide, partially filled, crater.

On the NNW lower flank of the massif, two small mafic scoria cones and associated lavas rest on top of the pre-Cóndor deposits (NW mafic center; Fig. 9). Their degree of preservation suggests that this center is older than the Cóndor stage.

The Cóndor stage consists of a great number of well-preserved blocky lava flows partially covering the pre-Cóndor deposits and extending beyond them (Cóndor stage; Figs. 9 and 10). The flows make up the western flank, most of the southern flank, and parts of the eastern flank of the volcano (Fig. 9). The summit region has four small (0.1 to 0.35 km diameters) craters aligned NNW-SSE (parallel to the elongation of the whole massif) and seems to be blanketed by scoria and pyroclastic deposits (Summit region; Fig. 9). Three other vents are present on the upper SE flank (Fig. 9). Lava flows seem to have filled the pre-Cóndor scarps and at places overpassed their rims. Towards the west, flows travelled ca. 9 km until reaching the foot of the Laguna Escondida volcano. Towards the east, flows travelled down the Laguna Amarga caldera floor and reached distances of up to 17 km from the summit region; individual flows on both flanks reach lengths of 9 km. Based on their morphologies and stratigraphic positions, the Cóndor stage lava flows can be separated into three groups. Lava flows 1 are the oldest and are the farthest-reaching flows towards the E and NE (Figs. 9 and 10). Lava flows 2 consist of two large flows on the E and S flanks and partially buried flow remnants on the SW and W flanks (Figs. 9 and 10). Lava flows 3 are the youngest and most abundant, covering most of the W and NW flanks and parts of the NE and SE flanks (Figs. 9 and 10). They can be sub-divided into lava flows 3a and 3b, based on their general appearance; lava flows 3b both cover and are covered by lava flows 3a. Lava flows 3a are the main type and are dark-colored and thinner. Lava flows 3b are light-colored and thicker; the larger of these descends the NE flank (Figs. 9 and 10), whereas the smaller forms a short coulée just south of the summit region (Fig. 9).

All volcanic products of El Cóndor belong to the high-K calc-alkaline series. The pre-Cóndor stage lavas are mostly

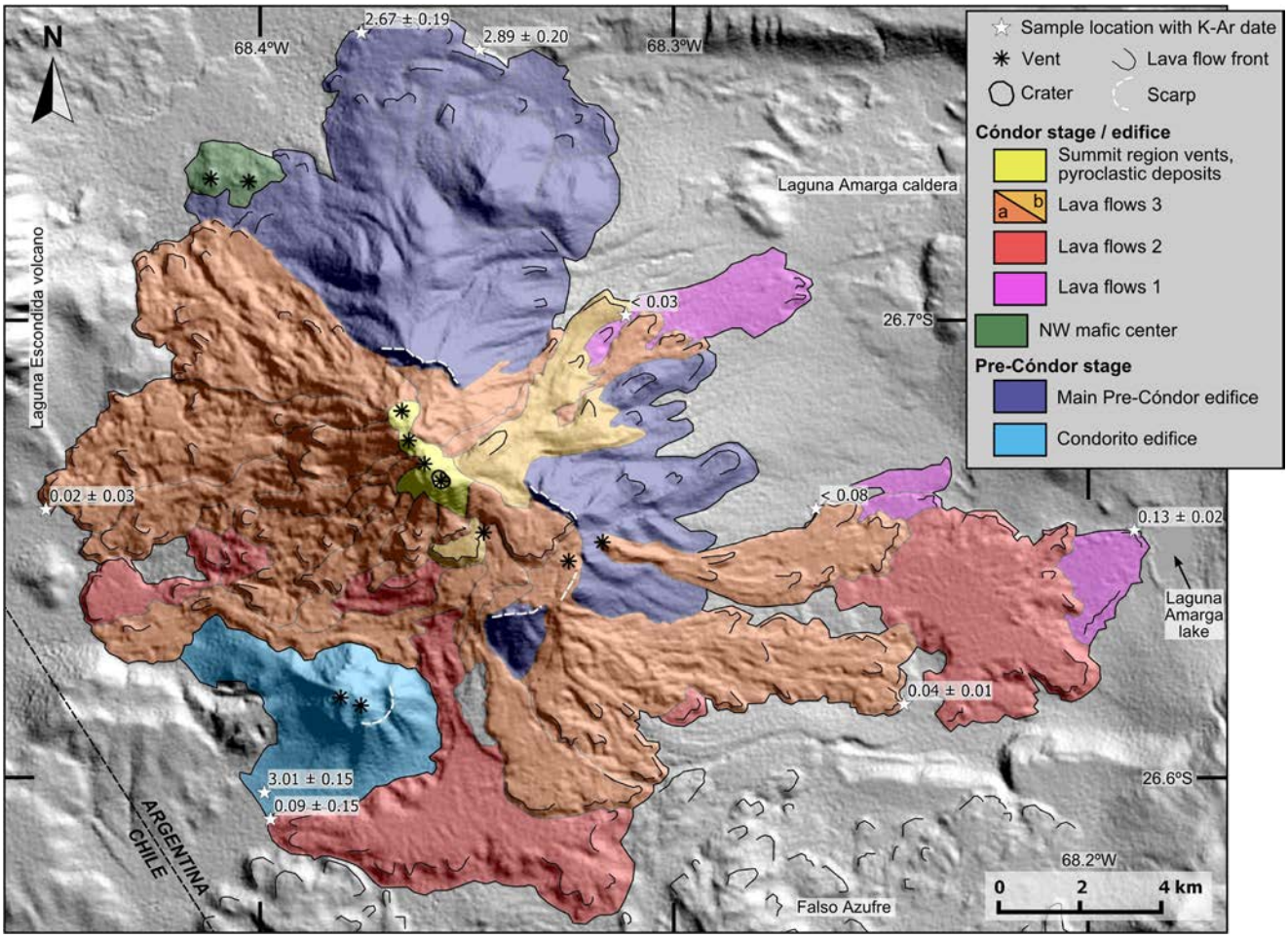

Fig. 9 SRTM 30 m DEM-derived shaded relief image of El Cóndor volcano showing volcanic units and features and new K-Ar ages

andesites, except for one dacitic flow on the lower northern flank. The Cóndor stage lavas are mainly trachyandesites, but also trachydacites (Fig. 3; Table 2).

K-Ar ages

There are no previous published ages for El Cóndor. Here we present nine new K-Ar ages (Table 3; Figs. 4 and 9). Three ages are of the pre-Cóndor stage lavas (Fig. 9). The oldest age of 3.01 ± 0.15 Ma is of an andesitic lava on the SW flank of the Condorito edifice. The other two ages, 2.67 ± 0.19 and 2.89 ± 0.20 Ma, are of andesitic and dacitic flow fronts on the northern lower flank.

The remaining six ages are of the Cóndor stage lava flows. The oldest dated sample, 0.13 ± 0.02 Ma, corresponds to the trachyandesitic lava flow 1 that is the farthest-reaching flow of the volcano, located next to the small Laguna Amarga lake (Figs. 9 and 10). The large, trachydacitic lava flow 2 on the southern flank gave an uncertain age of 0.09 ± 0.15 Ma (Fig. 9). Three ages are of lava flows 3a; two are trachyandesitic flows located on the SE flank, giving ages of 0.04 ± 0.01 and < 0.08 Ma, and the third is a trachydacitic flow on the western flank that gave an uncertain age of 0.02 ± 0.03 Ma (Fig. 9). Finally, the trachydacitic lava flow 3b on the NE flank gave an age of < 0.03 Ma (Fig. 9). Most of these ages have large errors because of the difficulty in obtaining

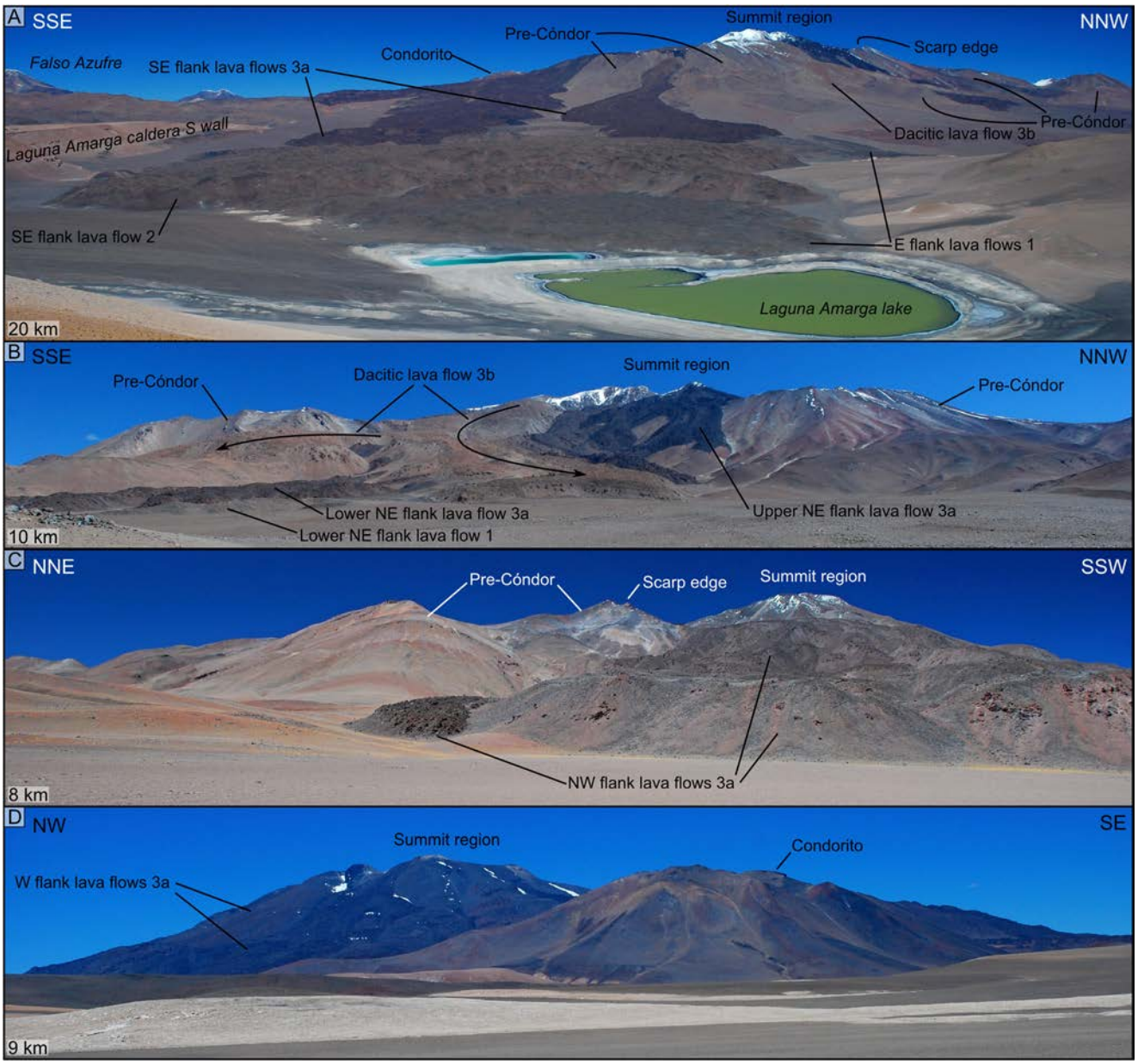

Fig. 10 Panoramic views of El Cóndor volcano from **a** East, **b** Northeast, **c** Northwest and **d** Southwest. Values at the lower left of each photograph are the approximate horizontal distances covered by the images

Table 4 Volumes, absolute ages, lifespans and average growth rates of Incahuasi, Falso Azufre, and El Cóndor volcanoes and of their main units

	Height	Area	Volume[a]	Absolute ages[b]		Lifespan[c]	Growth rate (km^3/ka)	
	(km)	(km^2)	(km^3)	Number	Age range (Ma)	(Ma)	Average	Range[d]
Incahuasi								
Total	2.0	207	62 ± 6	9	1.57 ± 0.10–0.35 ± 0.03	1.22 ± 0.13	0.05	0.04–0.06
Total (w/o NE mafic center)	2.0	166	61 ± 5	8	1.57 ± 0.10–0.71 ± 0.08	0.86 ± 0.18	0.07	0.05–0.10
Main edifice	1.9	128	57 ± 6	6	1.57 ± 0.10–0.71 ± 0.08	–	–	–
Lava dome	0.6	20	3.2 ± 0.4	1	0.76 ± 0.09	–	–	–
SE lava field	0.2	18	0.9 ± 0.4	1	0.74 ± 0.05	–	–	–
NE mafic center	0.3	41	0.8 ± 0.4	1	0.35 ± 0.03	–	–	–
Falso Azufre								
Total	1.2	387	98 ± 12	18	3.5 ± 0.7–0.16 ± 0.08	–	–	–
Kunstmann edifice	0.3	31	15 ± 2	3	3.5 ± 0.7–2.53 ± 0.24	–	–	–
SW edifice	0.2	6	0.3 ± 0.1	0	–	–	–	–
Quaternary Falso Azufre	1.1	350	83 ± 18	15	0.91 ± 0.22[e]–0.16 ± 0.08	0.75 ± 0.30	0.11	0.06–0.22
Falso Azufre s.s. edifice	1.1	202	55 ± 10	8	0.91 ± 0.18[e]–0.53 ± 0.09	–	–	–
Falso Azufre s.s. summit region	0.4	22	2.7 ± 0.7	0	–	–	–	–
Dos Conos edifice	1.1	109	26 ± 5	4	0.91 ± 0.22–0.37 ± 0.04	–	–	–
Dos Conos summit region	0.6	21	3.1 ± 0.6	1	0.37 ± 0.04	–	–	–
Eastern domes, coulées and flows	0.2	39	1.8 ± 1.2	3	0.26 ± 0.08–0.16 ± 0.08	–	–	–
Quaternary first pulse (flanks of Falso Azufre s.s. and Dos Conos)	–	268	75 ± 13	11	0.91 ± 0.22[e]–0.53 ± 0.09	0.38 ± 0.31	0.2	0.1–1.3
Quaternary second pulse (Eastern unit + summit regions)	–	82	8 ± 3	4	0.37 ± 0.04–0.16 ± 0.08	0.21 ± 0.12	0.04	0.02–0.11
El Cóndor								
Total	1.8	281	109 ± 8	9	3.01 ± 0.15–0.02 ± 0.03	–	–	–
Pre-Cóndor stage	1.0	87	68 ± 9	3	3.01 ± 0.15–2.67 ± 0.19	–	–	–
Main Pre-Cóndor remnants	1.0	70	> 19 ± 7	2	2.89 ± 0.20–2.67 ± 0.19	–	–	–
Condorito edifice	0.7	17	> 3.4 ± 0.9	1	3.01 ± 0.15	–	–	–
NW mafic center	0.1	2	0.07 ± 0.02	0	–	–	–	–
Cóndor stage edifice	1.2	192	41 ± 15	6	0.13 ± 0.02–0.02 ± 0.03	0.11 ± 0.04	0.4	0.2–0.7

[a] Volume estimates are given with an uncertainty value (σ_V); see text for details

[b] Both previously published and our new ages are considered

[c] Lifespan estimates are given with an uncertainty value (σ_L); see text for details

[d] Growth rate uncertainty range (σ_{GR}) spans the maximum and minimum possible growth rates; see text for details

[e] The age of 1.0 ± 0.4 Ma (Clavero et al. 2012) is not considered due to the large error

high-precision values in such young rocks with radiogenic determinations; ^{14}C dating is not an alternative as no organic material is interlayered in the lavas. Nevertheless, the obtained ages are a good approximation showing that these lavas are very young, as evidenced also by their pristine appearance.

Volumes, lifespans and growth rates

Table 4 shows the calculated volumes, lifespans and average growth rates for the three studied volcanoes and units, together with their associated uncertainties. We estimate only overall Quaternary growth rates for each of the three volcanoes, as the existing data is not sufficient to estimate neither the Pliocene growth rates of Falso Azufre and El Cóndor nor distinguish between different peak or background growth rates.

Incahuasi has an estimated total volume of 62 ± 6 km^3. The lava dome has an estimated volume of 3.2 ± 0.4 km^3, whereas the SE lava field and the NE mafic center are estimated at ca. 1 ± 0.4 km^3 each. Hence, the volume of the main edifice, excluding the three peripheral units, is estimated at 57 ± 6 km^3. The total lifespan of Incahuasi is 1.22 ± 0.13 Ma, or 0.86 ± 0.18 Ma if the NE mafic center is excluded. The average growth rate is estimated at 0.05 km^3/ka (σ_{GR} = 0.04–0.06 km^3/ka) considering all units, and 0.07 (σ_{GR} = 0.05–0.10 km^3/ka) excluding the NE mafic center.

The total volume of Falso Azufre is estimated at 98 ± 12 km^3. The minimum volume for the Kunstmann edifice,

considering only the exposed remnant, is 6 km^3, whereas a preferred volume of 15 ± 2 km^3 is obtained considering the lateral projection of the edifice below younger products. The volume of Falso Azufre excluding the Kunstmann edifice, i.e. the Quaternary Falso Azufre, is estimated at 83 ± 18 km^3. The volume of the SW edifice is estimated at 0.3 ± 0.1 km^3. The Falso Azufre *s.s.* and the Dos Conos edifices have estimated volumes of 55 ± 10 and 26 ± 5 km^3, respectively, whereas the volumes of their summit regions are estimated at ca. 3 ± 0.6 km^3 each. The Eastern unit has a volume estimated at 1.8 ± 1.2 km^3. The large temporal hiatus between the Kuntsmann edifice and the rest of Falso Azufre indicates two distinct stages. Quaternary activity of Falso Azufre, excluding the age of 1.0± 0.4 Ma of Clavero et al. (2012) due to its large error, spans between 0.91 ± 0.22 and 0.16 ± 0.08 Ma; the estimated lifespan is thus 0.75 ± 0.30 Ma. The average Quaternary growth rate is estimated at 0.11 km^3/ka, with a large σ_{GR} of 0.06–0.21 km^3/ka. The available ages suggest two Quaternary growth pulses: a main pulse between 0.91 ± 0.22 and 0.53 ± 0.09 Ma that constructed the bulk of both the Falso Azufre *s.s.* and the Dos Conos edifices and a secondary pulse $< 0.37 \pm 0.04$ Ma restricted to the summit regions and the Eastern unit. The volume of the first pulse is estimated at 75 ± 13 km^3, with a lifespan of ~ 0.4 Ma and an average growth rate of ~ 0.2 km^3/ka, whereas the second pulse has an estimated volume of 8 ± 3 km^3, a lifespan < 0.4 Ma and an average growth rate of < 0.1 km^3/ka.

The total volume of El Cóndor is estimated at 109 ± 8 km^3. The volumes of the pre-Cóndor and Cóndor stages are difficult to discriminate as they overlap considerably and the extent of the un-exposed pre-Cóndor deposits is unknown. The volumes of the exposed remnants of the main pre-Cóndor stage are estimated at 19 ± 7 km^3 and of the Condorito edifice at 3.4 ± 0.9 km^3, whereas a more realistic estimate, projecting the slopes of the pre-Cóndor remnants (including the Condorito edifice) below the Cóndor stage products, gives a volume of 68 ± 9 km^3. The estimated volume for the Cóndor stage is 41 ± 15 km^3. The Cóndor stage has a maximum age of 0.13 ± 0.02 Ma and minimum ages of 0.02 ± 0.03 and < 0.03 Ma; its lifespan is estimated at 0.11 ± 0.04 Ma and its average growth rate is estimated at 0.4 km^3/ka (σ_{GR} = 0.2–0.7 km^3/ka).

Discussion

Eruptive histories of the studied volcanoes and their eruptive potential

Incahuasi

The main edifice of Incahuasi is a voluminous symmetrical cone built up by andesite-trachyandesite, and subordinate basaltic trachyandesite, lava flows emitted from one central vent. Our ages, together with previous ages, indicate that construction of the main edifice took place between ~ 1.6 and ~ 0.7 Ma at an average growth rate of ~ 0.07 km^3/ka. At 0.8–0.7 Ma, the locus of activity shifted from the main cone to the eastern flank, with the approximately coeval emplacement of the dacitic lava dome and the SE lava field. However, the undated but pristine-looking stubby coulées on the summit region and a couple of well-preserved flows on the S and SW flanks are possibly younger than the dated lavas of the main edifice, thus activity from the main cone may have continued after 0.7 Ma. The youngest activity recorded at Incahuasi is from the NE mafic center, with an age of 0.35 ± 0.03 Ma. However, mafic monogenetic volcanism in the region is considered mantle-derived, without significant magma stalling in the crust as in the case of the andesitic stratovolcanoes of the area (e.g. Drew et al. 2009), and hence the NE mafic center is probably unrelated to the evolution of the main Incahuasi edifice.

The main edifice of Incahuasi has been inactive since ~ 0.7 Ma and hence future activity seems unprobable. It can be considered a young extinct volcano following the classification of Szakács (1994), although future activity cannot be completely ruled out as other volcanoes in the CVZ have shown repose periods in the order of 1 Ma (e.g. Tutupaca; Samaniego et al. 2015), and also because there seems to be availability of magma in the area (Bianchi et al. 2013; Ward et al. 2017).

Falso Azufre

The evolution of Falso Azufre can be separated into two main stages. The older stage corresponds to the Kunstmann edifice remnant. The available ages between 3.5 ± 0.7 and 2.5 ± 0.2 Ma are much older than all other ages, suggesting that the older stage is an unrelated volcanic episode, on top of which grew the modern Falso Azufre complex. The Kunstmann edifice seems to have consisted of a rather simple cone formed by andesitic lavas; its activity possibly ended with the formation of the large summit scarp that can be ascribed to a partially preserved crater or a collapse event. The volume of 15 ± 2 km^3 for this older stage is possibly an underestimate, as deposits may be buried below the products of the newer stage. The undated SW edifice may have been part of this older stage or else it is younger, but formed before the Falso Azufre *s.s.* and Dos Conos edifices.

The younger and main stage of activity at Falso Azufre is < 1.1 Ma. Considering the minimum age of 0.16 ± 0.08 Ma, the average growth rate of Falso Azufre's main stage is ~ 0.1 km^3/ka. This stage can be sub-divided into two pulses. The first pulse, between ~ 0.9 and ~ 0.5 Ma, constructed the bulk of the massif, including both the Falso Azufre *s.s.* and the Dos Conos edifices, at an estimated growth rate of ~ 0.2 km^3/ka.

This pulse consisted in the emplacement of andesitic-trachyandesitic lava flows on all flanks of the massif. The elongated, arcuate shape of the massif and the many aligned vents suggest a strong structural control during this time, with migration of activity along a NW-SE trend on the western part of the massif and along an ENE-WSW trend on the eastern part.

The second pulse is < 0.4 Ma and was restricted to the summit region of the Dos Conos edifice (possibly also the summit region of Falso Azufre *s.s.*) and the eastern portion of the massif and seems to be related to ENE-WSW trending structures. Short andesitic lava flows built the Dos Conos summit region, whereas dacitic domes and coulées and andesitic lava flows were emplaced on the eastern flank of the massif. Although not dated, the small lava flows and the pyroclastic deposits located at the Falso Azufre *s.s.* summit region are possibly also part of this younger pulse. The youngest activity seems to be that of the five small domes, three of which intrude the lava flow dated at 0.16 ± 0.08 Ma (Fig. 7). The average growth rate of this second pulse was < 0.1 km^3/ka, hence marking a decrease in productivity.

Available ages of Falso Azufre indicate it is a young extinct volcano following Szakács (1994). However, considering the age uncertainties and the absence of absolute ages for stratigraphically younger domes and for the pyroclastic deposits on the Falso Azufre *s.s.* summit region, the second pulse of activity possibly extends to < 0.1 Ma and could still be ongoing.

El Cóndor

Similarly to Falso Azufre, El Cóndor was constructed in two main stages separated by a long hiatus or repose period. However, at El Cóndor, the older pre-Cóndor stage remnants have a widespread distribution that suggests a large edifice built up at approximately the same location as the present El Cóndor edifice. Pre-Cóndor activity seems to have been centered around a large summit region which sourced andesitic lava flows that form the remnants to the east and north. Peripheral andesitic and dacitic lava flows and domes were emplaced on the northern flank, and a distinct but coalescing andesitic cone, Condorito, grew to the SW. The large scarps at the summit region of the pre-Cóndor edifice suggest a catastrophic, possibly final collapse event, after which activity ceased. Three ages constrain the pre-Cóndor stage, including Condorito, to 3.0 ± 0.2 to 2.7 ± 0.2 Ma.

The mafic center on the NW flank of El Cóndor intrudes the pre-Cóndor deposits, and hence is younger than ~ 2.7 Ma. Its degree of preservation suggests that it is older than the Cóndor stage.

The modern Cóndor stage built the present massif on top of the pre-Cóndor edifice, partially covering it. It consists of lava flows sourced mainly from a summit region formed by vents aligned NNW-SSE, suggesting a structural control. Lavas of the Cóndor stage are trachyandesitic and trachydacitic, hence suggesting a shift to more alkali-rich compositions in comparison with the pre-Cóndor stage. The obtained ages constrain the Cóndor stage to < 0.15 Ma, with an overall growth rate of ~ 0.4 km^3/ka.

Cóndor stage activity continued until at least ~ 0.02 Ma, although the age uncertainties hinder further precision. Furthermore, stratigraphically younger undated lavas in the summit region are < 0.02 Ma and could very well be Holocene in age. Hence, the main constructive phase could still be ongoing. El Cóndor can be considered a dormant active volcano following Szakács (1994) and has the highest potential for future eruptions of the three studied volcanoes.

Hazards related to the three studied volcanoes

Incahuasi, Falso Azufre and El Cóndor volcanoes are located far from urban areas and thus imply very low to null direct threat to populations. However, a main international road passes just south of Falso Azufre and the small settlement of Las Grutas is located nearby (Figs. 2 and 7). Although pyroclastic deposits are only recognized through satellite image analysis at the summit regions of Falso Azufre and El Cóndor, their occurence in unsurveyed areas or as deposits buried by lava flows cannot be ruled out. Hence, future explosive activity is not excluded and could affect several aerial routes passing east of the area (e.g. Buenos Aires-Lima; most domestic flights connecting with Salta, Tucumán and Jujuy in northwest Argentina), as winds flow from west to east at these latitudes.

Comparison of volumes and ages with other volcanoes from the Paso San Francisco region

The largest Quaternary volcanoes of the Paso San Francisco region are elongated massifs (Table 1), most of which show two distinct stages of activity separated by a long hiatus. This is the case of Falso Azufre, El Cóndor, Azufrera de Los Cuyanos-Piedra Parada and Tres Cruces (Table 1; Fig. 2). These four volcanoes are made of Upper Miocene or Pliocene remnants and Quaternary edifices constructed on top. Incahuasi in turn is by far the largest Quaternary conical volcano of the region (Table 1).

The older stages of activity of Falso Azufre (~ 2.5–3.5 Ma) and El Cóndor (~ 2.7–3.0 Ma) are coeval to several Pliocene volcanoes to the west (Fig. 2). Taken together, these edifices attest the abundant volcanism during the Pliocene on an already well-established frontal arc (e.g. Kay and Mpodozis 2002; Kay and Coira 2009).

Available Quaternary K-Ar and Ar-Ar ages in the Paso San Francisco region are mostly < 1.7 Ma (Table 1), suggesting a lull in activity during the Early Pleistocene which coincides with the hiatus at Falso Azufre and El Cóndor. Main activity at Incahuasi between ca. 1.6 and 0.7 Ma coincides with activity

Table 5 Volumes, lifespans and average growth rates of volcanoes from the Central Volcanic Zone of the Andes and world-wide examples from other arcs

Volcano	Volume (km^3)	Lifespan (Ma)	Growth rates (km^3/ka)		References
			Average	Range	
Central Volcanic Zone of the Andes					
Ampato-Sabancaya	44–54	0.44 ± 0.01	0.11	0.10–0.13	Samaniego et al. (2016)
Ampato	38–42	0.42 ± 0.01	0.10	0.09–0.10	
Sabancaya	6–10	0.012 ± 0.001	0.65	0.47–0.85	
El Misti	70–83	0.11 ± 0.01	0.68	0.59–0.78	Thouret et al. (2001)
Ubinas	56	0.38 ± 0.03	0.15	0.13–0.18	Thouret et al. (2005)
Taapaca	35	1.46 ± 0.07	0.02	0.02–0.03	Clavero et al. (2004b)
Parinacota	46 ± 5	0.16 ± 0.01	0.29	0.24–0.33	Hora et al. (2007)
Irruputuncu	4	0.26 ± 0.05	0.02	0.01–0.02	Rodríguez et al. (2015)
Aucanquilcha	38	0.80 ± 0.06	0.05	0.04–0.06	Klemetti and Grunder (2008)
Ollagüe	80–90	1.10 ± 0.12	0.08	0.07–0.09	Feeley et al. (1993); Wörner et al. (2000); Clavero et al. (2004a); Vezzoli et al. (2008)
Uturuncu	50	0.80 ± 0.01	0.06	0.06–0.07	Muir et al. (2015)
Láscar (edifice)	15	< 0.043	0.35	0.3–0.4	Gardeweg et al. (1998)
Láscar (erupted)	30–40		0.81	0.7–0-9	
Llullaillaco	37[a]	1.45 ± 0.41	0.03	0.02–0.04	Gardeweg et al. (1984); Richards and Villeneuve (2001)
Azufrera de Los Cuyanos	36[a]	1.05 ± 0.09	0.03	0.03–0.04	Polanco et al. (2014)
Ojos del Salado	54[a]	1.53 ± 0.13	0.04	0.03–0.04	González-Ferrán et al. (1985); Mpodozis et al. (1996); Gardeweg et al. (1997)
Tres Cruces (Quaternary)[b]	38[a]	2.07 ± 0.32	0.02	0.01–0.02	Mpodozis et al. (1996); Gardeweg et al. (2000)
El Cóndor (Quaternary)[b]	41 ± 15	0.11 ± 0.04	0.4	0.2–0.7	This study
Falso Azufre (Quaternary)[b]	83 ± 18	0.75 ± 0.30	0.11	0.06–0.22	This study; Zentilli (1974); Mpodozis et al. (1996); Clavero et al. (2012)
Incahuasi (total)[c]	62 ± 6	1.22 ± 0.13	0.05	0.04–0.06	This study; González-Ferrán et al. (1985); Mpodozis et al. (1996)
Incahuasi (w/o NE mafic center)[c]	61 ± 5	0.86 ± 0.18	0.07	0.05–0.10	
Volcanoes from other arcs					
New Zealand					
Tongariro	60	0.27 ± 0.02	0.22	0.18–0.26	Hobden et al. (1999)
Ruapehu	150	0.21 ± 0.03	0.73	0.58–0.93	Gamble et al. (2003); Conway et al. (2016)
Java					
Sundoro	4.4	0.034	0.13	0.12–0.14	Prambada et al. (2016)
Kyushu					
Unzen	128	0.44 ± 0.02	0.29	0.25–0.34	Hoshizumi et al. (1999)
Aleutians					
Tanaga volcanic cluster	97	0.30 ± 0.01	0.33	0.28–0.38	Jicha et al. (2012)
Seguam Island	79	0.32 ± 0.03	0.25	0.20–0.30	Jicha and Singer (2006)
Mount Katmai (erupted)	70 ± 18	0.089 ± 0.013	0.79	0.51–1.16	Hildreth et al. (2003b)
Mount Mageik (edifice)	20	0.093 ± 0.008	0.22	0.18–0.26	Hildreth et al. (2003b)
Mount Mageik (erupted)	30		0.32	0.27–0.39	
Trident (erupted)	22 ± 3	0.14 ± 0.01	0.15	0.13–0.19	Hildreth et al. (2003b)
Mount Griggs (edifice)	20–25	0.29 ± 0.01	0.08	0.07–0.09	Hildreth et al. (2003b)
Mount Griggs (erupted)	35 ± 5		0.12	0.10–0.14	
Cascades					
Mount Baker stratocone	15	0.043 ± 0.005	0.35	0.25–0.47	Hildreth et al. (2003a)

Table 5 (continued)

Volcano	Volume (km^3)	Lifespan (Ma)	Growth rates (km^3/ka)		References
			Average	Range	
Mount Adams stratocone	200	0.50 ± 0.02	0.40	0.35–0.45	Hildreth and Lanphere (1994)
North Sister	40	0.45 ± 0.15	0.09	0.06–0.15	Schmidt and Grunder (2009)
South sister	17–20	0.05 ± 0.010	0.38	0.29–0.51	Fierstein et al. (2011)
Mount Mazama (erupted)	176	0.42 ± 0.01	0.42	0.37–0.47	Bacon and Lanphere (2006)
Trans-Mexican					
Ceboruco	51 ± 2.5	0.10 ± 0.02	0.51	0.40–0.67	Frey et al. (2004)
Tequila	31 ± 2.1	0.04 ± 0.02	0.81	0.51–1.74	Lewis-Kenedi et al. (2005)
Tancítaro	97 ± 3	0.56 ± 0.06	0.17	0.15–0.20	Ownby et al. (2007)
Central America					
Santa María	16	0.10 ± 0.02	0.16	0.12–0.21	Escobar-Wolf et al. (2010)
Santa María (pre-1902)	8	0.07 ± 0.02	0.12	0.08–0.19	
Northern Andes					
Guagua Pichincha	36–38	0.055 ± 0.005	0.67	0.60–0.76	Robin et al. (2010)
Chimborazo (edifice)	72–83	~0.12	0.65	0.55–0.77	Samaniego et al. (2012)
Chimborazo (erupted)	58–80		0.58	0.44–0.74	
Southern Andes					
Tatara-San Pedro	23.5	0.09 ± 0.02	0.26	0.20–0.36	Singer et al. (1997)
Puyehue-Cordón Caulle	131	0.31 ± 0.01	0.42	0.36–0.48	Singer et al. (2008)
Puyehue	76–104		0.29	0.23–0.35	

Lifespans and lifespan uncertainties calculated from maximum and minimum available ages and their errors; for volcanoes with historical activity minimum ages of zero were considered

For volcanoes lacking a volume uncertainty or range value, a volume uncertainty of 10% was assumed for the estimation of the growth rate uncertainty ranges

[a] Volumes estimated by us using the SRTM DEM

[b] Only the Quaternary volumes and lifespans are considered

[c] Values including and excluding the NE mafic center

at San Francisco, Cerro Bertrand, El Solo and El Muertito, whereas activity at Falso Azufre between ca. 0.9 and 0.2 Ma coincides with activity at Azufrera de Los Cuyanos, El Fraile and El Muerto (Table 1). Available ages for Tres Cruces, Ojos del Salado and Sierra Nevada span the activity of both Incahuasi and Falso Azufre (Table 1). Activity at El Cóndor of < 0.15 Ma is younger than at most other centers. The only other records of activity within this time span are two Ar-Ar ages at the Tres Cruces massif of 0.028 ± 0.022 and 0.068 ± 0.009 Ma (Gardeweg et al. 2000).

Comparison of volumes, lifespans and average growth rates with other Quaternary volcanoes from the Central Andes and from other arcs

Arc volcanoes tend to have lifespans below 1 Ma, although some record activity exceeding 1 Ma (see Table 5). They commonly grow in spurts, with peaks of activity, or cone-building episodes, separated by repose periods with minor or no activity (e.g. Hildreth and Lanphere 1994; Davidson and de Silva 2000; Lewis-Kenedi et al. 2005; Singer et al. 2008). Cone-building episodes usually last < 100 ka, with growth rates above 0.1 km^3/ka and up to 10 km^3/ka (e.g. Singer et al. 2008 and references therein). Repose periods can last longer, up to 400 ka (e.g. Hildreth and Lanphere 1994) and possibly even more in CVZ volcanoes, and can show background activity that is usually < 0.1 km^3/ka (Hildreth and Lanphere 1994; Hildreth et al. 2003a). However, some volcanoes show almost continuous activity with no or very short repose periods (e.g. Jicha et al. 2012). Considering their total lifespans and volumes, average growth rates of arc volcanoes may vary significantly, but are generally in the order of 0.05 to 1 km^3/ka (Table 5). Estimating growth rates is complicated by the uncertainties linked to both age determinations and volume estimations. Volume uncertainties are particularly critical, and can be very high depending on the degree of erosion,

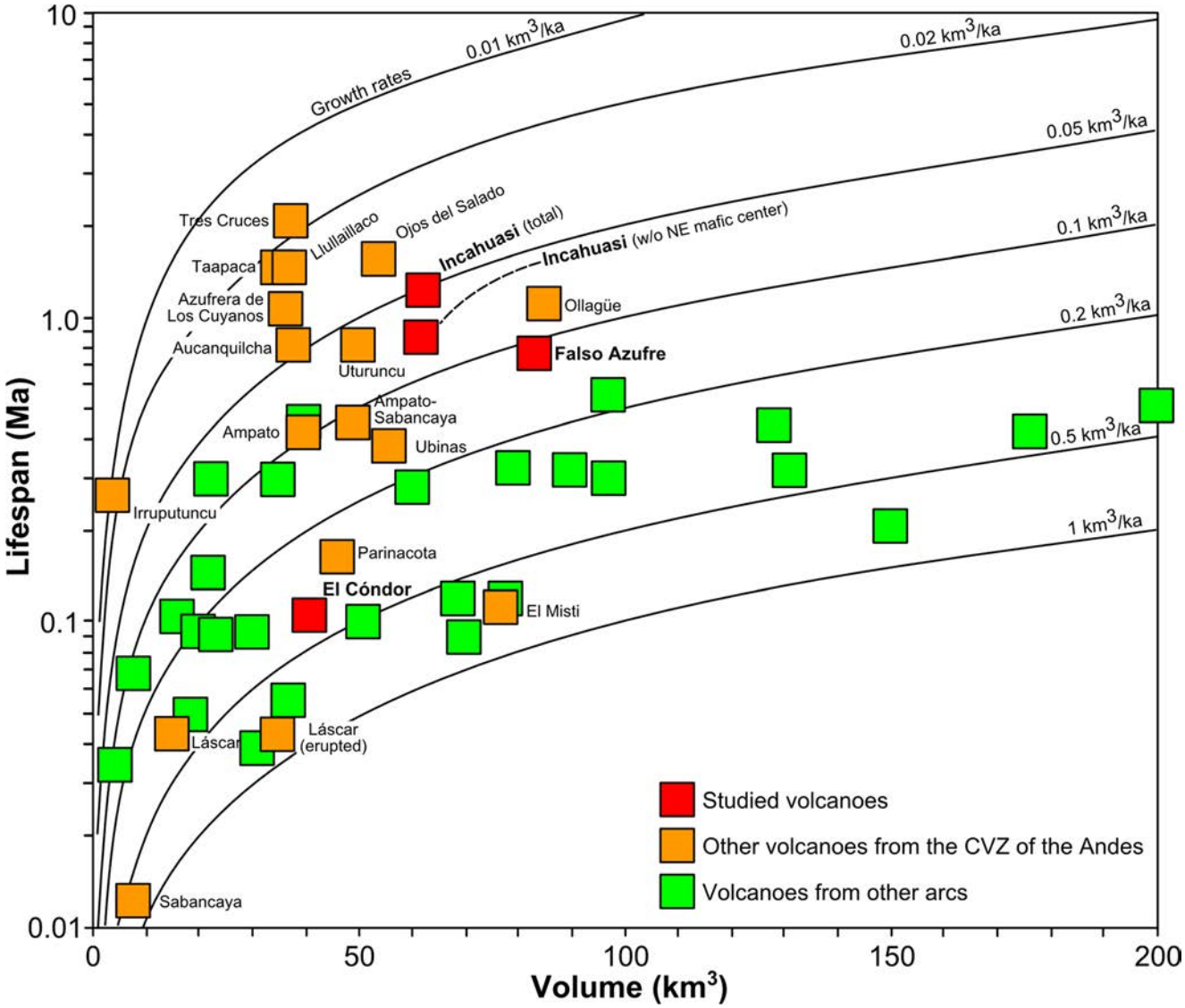

Fig. 11 Plot of volume vs. lifespan for volcanoes of the Central Volcanic Zone of the Andes and world-wide examples from other arcs. For Falso Azufre and El Cóndor, only the Quaternary volumes and lifespans are considered; for Incahuasi, values are plotted both including and excluding the NE mafic center

notably glacial (e.g. Singer et al. 1997; Hildreth et al. 2003b; Schmidt and Grunder 2009), and/or the amount of pyroclastic products not preserved within the edifice (e.g. Gardeweg et al. 1998; Bacon and Lanphere 2006). Hence, caution should be used when estimating and comparing growth rates, and the type of growth rate that is being measured (e.g. of the whole volcano lifespan, of a stage in the volcano evolution, of a peak cone-building episode) should always be taken into account (e.g. Hildreth and Lanphere 1994; Singer et al. 2008).

Volumes of individual Quaternary volcanoes from the CVZ range from 4 to ca. 100 km^3 (Table 5; Fig. 11), although a few other volcanoes not considered here, because they lack detailed studies, have volumes > 100 km^3 (e.g. Coropuna, Chachani, San Pedro-San Pablo, Pular-Pajonales; Grosse et al. 2014a). Ollagüe, Falso Azufre and El Misti are the largest volcanoes, with volumes between 70 and 90 km^3. Most of the considered volcanoes have volumes between 35 and 60 km^3, and the largest of these is Incahuasi. Lifespans range from 0.01 to > 1 Ma (0.7 Ma on average). The lifespans of Incahuasi (~ 0.9 Ma, excluding the NE mafic center) and Falso Azufre (~ 0.8 Ma) are around average, whereas the current lifespan of El Cóndor (< 0.15 Ma) is much shorter than average, similar to El Misti. The average growth rates range between 0.02 to 0.8 km^3/ka, with a median average of 0.08 km^3/ka. The estimated growth rates for Incahuasi (~ 0.05 or ~ 0.07 km^3/ka) and Falso Azufre (~ 0.1 km^3/ka) are around average. The growth rate of El Cóndor (~ 0.4 km^3/ka) is among the five highest of the CVZ volcanoes, together with Láscar, El Misti, Parinacota and Sabancaya. These five volcanoes are the youngest, have the shortest lifespans and have not

yet experienced a considerable repose period; they are probably undergoing a main growth phase and hence their growth rates can be considered peak growth rates.

The average lifespan of the selected Quaternary volcanoes from other arcs is 0.2 Ma, and the median average growth rate is 0.3 km^3/ka. Hence, the Quaternary growth rate of El Cóndor is similar to the average from other arcs, whereas those of Falso Azufre and Incahuasi are below average rates. CVZ volcanoes tend to have longer lifespans and lower growth rates (and hence probably lower eruptive frequencies) compared to volcanoes from other arcs (Table 5; Fig. 11), suggesting fundamental differences between the CVZ and other arcs that could be related to the extremely thick crust of the CVZ (> 70 km, e.g. Beck et al. 1996) and/or differences in the subduction dynamics (e.g. Acocella and Funiciello 2010; Chaussard and Amelung 2014). A thicker crust may stall magma ascent (e.g. Trumbull et al. 2006; Chaussard and Amelung 2014), producing longer lifespans and lower overall growth rates, as could be the case for most CVZ volcanoes, including Incahuasi and Falso Azufre. However, higher or peak growth rates are still possible in the CVZ as shown by the younger volcanoes including El Cóndor. Higher rates may occur at volcanoes related to crustal-scale structures that act as ascent paths (e.g. Wörner et al. 2000), as could have happened at for example Parinacota, where a link with a magma focussing lineament has been suggested by Hora et al. (2007).

Conclusions

Incahuasi, Falso Azufre and El Cóndor are high-K calc-alkaline, mainly andesitic-trachyandesitic volcanoes, with subordinate dacitic-trachydacitic and rare basaltic (trachy)andesite products. Activity at the three volcanoes has been mainly effusive, consisting mostly of the emplacement of lava flows, but also of coulées and domes, particularly during younger more felsic phases. Small pyroclastic deposits are only observed at the summit regions of Falso Azufre and El Cóndor.

Activity at Incahuasi was concentrated at a single central vent during its main constructive phase, from ~ 1.6 to 0.7 Ma, at a rate of ~ 0.07 km^3/ka. The end of this phase was marked by the emplacement of a large dacitic lava dome and a small lava field on the eastern flanks, and possibly also felsic coulées at the summit region. A mafic center formed at ~ 0.35 Ma, probably related to a regional event of mafic monogenetic volcanism following a NNE-SSW trend.

Falso Azufre and El Cóndor show two stages of activity separated by long hiatus of ~ 1.6 and ~ 2.6 Ma, respectively. The older stages are Upper Pliocene. At Falso Azufre, the younger stage is < 1.1 Ma and had an average growth rate of ~ 0.1 km^3/ka. A main pulse between ca. 0.9 and 0.5 Ma constructed most of the massif and was followed by a minor more felsic pulse < 0.4 Ma, restricted to the eastern flank and the summit regions. At El Cóndor, the younger stage is < 0.15 Ma. It is among the youngest recorded activity in the region and the estimated growth rate of ~ 0.4 km^3/ka is among the highest reported for composite volcanoes of the CVZ.

Most CVZ volcanoes, including Incahuasi and Falso Azufre, tend to have longer lifespans and lower average growth rates compared to volcanoes from other arcs, which could be related to the extremely thick crust in the CVZ and/or different subduction dynamics. El Cóndor and a few other young volcanoes from the CVZ have higher growth rates, similar to those of other arcs; they have not experienced significant repose periods and are possibly still undergoing their main growth phases.

The three studied volcanoes are at different stages in their evolutions and hence have different eruptive potentials. Incahuasi has the lowest long-term eruptive potential, as the build-up stage ended at ~ 0.7 Ma and no activity from the main cone has been recorded since then. At Falso Azufre, the main constructive phase seems to have ended, but a subsequent minor more felsic phase is possibly ongoing; its long-term eruptive potential is intermediate. El Cóndor has had the most recent activity and its main constructive phase may still be ongoing; hence, it has the highest long-term eruptive potential. The eruptive chronology of the three volcanoes plus the recent identification of a large magma body in the region (Ward et al. 2017) calls the attention to the hazards that they may imply. Finally, their eruptive histories may give insights on the past and/or future behavior of similar volcanoes in other parts of the CVZ that pose a greater threat.

Acknowledgements This work was funded by CONICET (Consejo Nacional de Investigaciones Científicas y Técnicas, Argentina) project PIP IU 286, Fundación Miguel Lillo (Argentina), through a scholarship awarded to PG by the CONICET–JSPS (Japan Society for the Promotion of Science) International Cooperation Program, and by the JSPS KAKENHI grant 15H02630 awarded to YO. SG thanks the project of CONICET (PUE IBIGEO). Mie Ichihara is thanked for her assistance and hospitality during PG's stay in Japan. N. Hokanishi is thanked for her support during XRF analysis. PG is very grateful to Constantino Grosse for his invaluable assistance and companionship in the field. We thank Valerio Acocella and Shanaka de Silva for their thourough reviews of a previous version. Two anonymous reviewers and Associate Editor Valerio Acocella provided insightful comments that greatly improved the manuscript.

References

Acocella V, Funiciello F (2010) Kinematic setting and structural control of arc volcanism. Earth Planet Sc Lett 289:43–53

Acocella V, Gioncada A, Omarini R, Riller U, Mazzuoli R, Vezzoli L (2011) Tectonomagmatic characteristics of the back-arc portion of the Calama–Olacapato–El Toro fault zone, Central Andes. Tectonics 30:TC3005

Bacon CR, Lanphere MA (2006) Eruptive history and geochronology of Mount Mazama and the Crater Lake region, Oregon. Geol Soc Am Bull 118:1331–1359

Báez W, Arnosio M, Chiodi A, Ortiz-Yañes A, Viramonte JG, Bustos E, Giordano G, López JF (2015) Estratigrafía y evolución del Complejo Volcánico Cerro Blanco, Puna Austral, Argentina. Rev Mex Cienc Geol 31:29–49

Baker PE, González-Ferrán O, Rex DC (1987) Geology and geochemistry of the Ojos del Salado volcanic region, Chile. J Geol Soc Lond 144:85–96

Barazangi M, Isacks BL (1976) Spatial distribution of earthquakes and subduction of the Nazca plate beneath South America. Geology 4: 686–692

Beck SL, Zandt G, Myers SC, Wallace TC, Silver PG, Drake L (1996) Crustal-thickness variations in the Central Andes. Geology 24:407–410

Bianchi M, Heit B, Jakovlev A, Yuan X, Kay SM, Sandvol E, Alonso RN, Coira B, Brown L, Kind R, Comte D (2013) Teleseismic tomography of the southern Puna plateau in Argentina and adjacent regions. Tectonophysics 586:65–83

Biggs J, Ebmeier SK, Aspinall WP, Lu Z, Pritchard ME, Sparks RSJ, Mather T (2014) Global link between deformation and volcanic eruption quantified by satellite imagery. Nat Commun 5:3471–3471

Brown SK, Loughlin SC, Sparks RSJ, Vye-Brown C, Barcalay J, Calder E, Cotrell E, Jolly G, Komorowski J-C, Mandeville C, Newhall C, Palma J, Potter S, Valentine G (2015) Global volcanic hazard and risk. In: Loughlin SC, Sparks RSJ, Brown SK, Jenkins SF, Vye-Brown C (eds) Global volcanic hazards and risk. Cambridge University Press, Cambridge, pp 81–172

Cahill T, Isacks BL (1992) Seismicity and shape of the subducted Nazca plate. J Geophys Res Solid Earth 97:17503–17529

Carniel R (2014) Characterization of volcanic regimes and identification of significant transitions using geophysical data: a review. B Volcanol 76:848

Chaussard E, Amelung F (2014) Regional controls on magma ascent and storage in volcanic arcs. Geochem Geophys Geosyst 15:1407–1418

Chernicoff CJ, Richards JP, Zappettini EO (2002) Crustal lineament control on magmatism and mineralization in northwestern Argentina: geological, geophysical, and remote sensing evidence. Ore Geol Rev 21:127–155

Clavero J, Mpodozis C, Gardeweg M (1997) Mapa geológico del área del Salar de Wheelwright, Región de Atacama (Escala 1:100.000). Servicio Nacional de Geología y Minería de Chile

Clavero J, Polanco E, Godoy E, Aguilar G, Sparks S, van Wyk de Vries B, Pérez de Arce C, Matthews S (2004a) Substrata influence in the transport and emplacement mechanism of the Ollagüe debris avalanche (northern Chile). Acta Vulcanol 16:59–76

Clavero JE, Sparks RSJ, Pringle MS, Polanco E, Gardeweg MC (2004b) Evolution and volcanic hazards of Taapaca volcanic complex, Central Andes of northern Chile. J Geol Soc Lond 161:603–618

Clavero J, Mpodozis C, Gardeweg M, Valenzuela M (2012) Geología de las áreas Laguna Wheelwright y Paso San Francisco, Región de Atacama (Escala 1:100.000). Servicio Nacional de Geología y Minería de Chile

Connor CB, McBirney AR, Furlan C (2006) What is the probability of explosive eruption at a long-dormant volcano? In: Mader HM, Coles SG, Connor CB, Connor LJ (eds) Statistics in volcanology, 1st edn. Spec Pub IAVCEI 1. Geol Soc London, pp 39–46

Conway CE, Leonard GS, Townsend DB, Calvert AT, Wilson CJ, Gamble JA, Eaves SR (2016) A high-resolution $^{40}Ar/^{39}Ar$ lava chronology and edifice construction history for Ruapehu volcano, New Zealand. J Volcanol Geotherm Res 327:152–179

Crosweller HS, Arora B, Brown SK, Cottrell E, Deligne NI, Guerrero NO, Hobbs L, Kiyosugi K, Loughlin SC, Lowndes J, Nayembil M, Siebert L, Sparks RSJ, Takarada S, Venzke E (2012) Global database on large magnitude explosive volcanic eruptions (LaMEVE). J Appl Volcanol 1:4

Davidson J, de Silva S (2000) Composite volcanoes. In: Sigurdsson H et al (eds) Encyclopedia of volcanoes. Academic Press, Cambridge, pp 663–681

de Silva S, Francis P (1991) Volcanoes of the Central Andes. Springer-Verlag, Berlin

Drew ST, Ducea MN, Schoenbohm LM (2009) Mafic volcanism on the Puna plateau, NW Argentina: implications for lithospheric composition and evolution with an emphasis on lithospheric foundering. Lithosphere 1:305–318

Escobar-Wolf RP, Diehl JF, Singer BS, Rose WI (2010) $^{40}Ar/^{39}Ar$ and paleomagnetic constraints on the evolution of Volcán de Santa María, Guatemala. Geol Soc Am Bull 122:757–771

Feeley TC, Davidson JP, Armendia A (1993) The volcanic and magmatic evolution of Volcán Ollagüe, a high-K, late Quaternary stratovolcano in the Andean Central Volcanic Zone. J Volcanol Geotherm Res 54:221–245

Fierstein J, Hildreth W, Calvert AT (2011) Eruptive history of South Sister, Oregon Cascades. J Volcanol Geotherm Res 207:145–179

Folkes CB, Wright HM, Cas RAF, de Silva SL, Lesti C, Viramonte JG (2011) A re-appraisal of the stratigraphy and volcanology of the Cerro Galán volcanic system, NW Argentina. B Volcanol 73: 1427–1454

Frey HM, Lange RA, Hall CM, Delgado-Granados H (2004) Magma eruption rates constrained by $^{40}Ar/^{39}Ar$ chronology and GIS for the Ceboruco-San Pedro volcanic field, western Mexico. Geol Soc Am Bull 116:259–276

Gamble JA, Price RC, Smith IEM, McIntosh WC, Dunbar NW (2003) $^{40}Ar/^{39}Ar$ geochronology of magmatic activity, magma flux and hazards at Ruapehu volcano, Taupo Volcanic Zone, New Zealand. J Volcanol Geotherm Res 120:271–287

Gardeweg M, Cornejo P, Davidson J (1984) Geologia del volcan Llullaillaco, Altiplano de Antofagasta, Chile (Andes Centrales). Rev Geol Chile 23:21–37

Gardeweg M, Mpodozis C, Clavero J, Cuitiño L (1997), Mapa geológico de la Hoja Nevado Ojos del Salado, Región de Atacama (Escala 1: 100.000). Servicio Nacional de Geología y Minería de Chile

Gardeweg MC, Sparks RSJ, Matthews SJ (1998) Evolution of Lascar volcano, northern Chile. J Geol Soc Lond 155:89–104

Gardeweg M, Clavero J, Mpodozis C, Pérez de Arce C, Villeneuve M (2000) El Macizo Tres Cruces: un complejo volcánico longevo y potencialmente activo en la Alta Cordillera de Copiapó, Chile. IX Congreso Geológico Chileno Actas 2:291–295

Gillot PY, Chiesa S, Pasquare G, Vezzoli L (1982) < 33,000-yr K-Ar dating of the volcano-tectonic horst of the isle of Ischia, Gulf of Naples. Nature 299:242–244

González-Ferrán O (1995) Volcanes de Chile. Instituto Geográfico Militar, Santiago

González-Ferrán O, Baker PE, Rex DC (1985) Tectonic-volcanic discontinuity at latitude 27° south, Andean range, associated with Nazca plate subduction. Tectonophysics 112:423–441

Goss AR, Kay SM, Mpodozis C, Singer BS (2009) The Incapillo Caldera and Dome Complex (~28° S, Central Andes): a stranded magma chamber over a dying arc. J Volcanol Geotherm Res 184:389–404

Goss AR, Kay SM, Mpodozis C (2013) Andean adakite-like high-Mg andesites on the northern edge of the Chilean–Pampean flat-slab (27–28.5°S) associated with frontal arc migration and fore-arc subduction erosion. J Petrol 54:2193–2234

Grosse P, van Wyk de Vries B, Petrinovic IA, Euillades PA, Alvarado G (2009) Morphometry and evolution of arc volcanoes. Geology 37: 651–654

Grosse P, van Wyk de Vries B, Euillades PA, Kervyn M, Petrinovic IA (2012) Systematic morphometric characterization of volcanic edifices using digital elevation models. Geomorphology 136:114–131

Grosse P, Euillades P, Euillades LD, vanWyk de Vries B (2014a) A global database of composite volcano morphometry. Bull Volcanol 76:784

Grosse P, Orihashi Y, Guzmán SR, Petrinovic IA (2014b) Volcanismo Cuaternario en la zona del Paso San Francisco, Catamarca. XIX Cong Geol Argentino, Abstract S24–2-6

Grosse P, Guzmán S, Petrinovic IA (2017) Volcanes compuestos cenozoicos del noroeste argentino. In: Muruaga CM, Grosse P (eds) Ciencias de la Tierra y Recursos Naturales del NOA. Relatorio del XX Cong Geol Argentino, Tucumán, pp 484–517

Guillou H, Van Vliet-Lanoë B, Guðmundsson A, Nomade S (2010) New unspiked K–Ar ages of Quaternary sub-glacial and sub-aerial volcanic activity in Iceland. Quat Geochronol 5:10–19

Guzmán S, Grosse P, Montero-López C, Hongn F, Pilger R, Petrinovic I, Seggiaro R, Aramayo A (2014) Spatial-temporal distribution of explosive volcanism in the 25-28°S segment of the Andean Central Volcanic Zone. Tectonophysics 636:170–189

Hildreth W, Lanphere MA (1994) Potassium-argon geochronology of a basalt-andesite-dacite arc system: the Mount Adams volcanic field, Cascade range of southern Washington. Geol Soc Am Bull 106: 1413–1429

Hildreth W, Fierstein J, Lanphere MA (2003a) Eruptive history and geochronology of the Mount Baker volcanic field, Washington. Geol Soc Am Bull 115:729–764

Hildreth W, Lanphere MA, Fierstein J (2003b) Geochronology and eruptive history of the Katmai volcanic cluster, Alaska peninsula. Earth Planet Sc Lett 214:93–114

Hobden BJ, Houghton BF, Davidson JP, Weaver SD (1999) Small and short-lived magma batches at composite volcanoes: time windows at Tongariro volcano, New Zealand. J Geol Soc Lond 156:865–868

Hora JM, Singer BS, Wörner G (2007) Volcano evolution and eruptive flux on the thick crust of the Andean Central Volcanic Zone: $^{40}Ar/^{39}Ar$ constraints from Volcán Parinacota, Chile. Geol Soc Am Bull 119:343–362

Hoshizumi H, Uto K, Watanabe K (1999) Geology and eruptive history of Unzen volcano, Shimabara peninsula, Kyushu, SW Japan. J Volcanol Geotherm Res 89:81–94

Jicha BR, Singer BS (2006) Volcanic history and magmatic evolution of Seguam Island, Aleutian Island arc, Alaska. Geol Soc Am Bull 118: 805–822

Jicha BR, Coombs ML, Calvert AT, Singer BS (2012) Geology and $^{40}Ar/^{39}Ar$ geochronology of the medium- to high-K Tanaga volcanic cluster, western Aleutians. Geol Soc Am Bull 124:842–856

Karátson D, Telbisz T, Wörner G (2012) Erosion rates and erosion patterns of Neogene to Quaternary stratovolcanoes in the Western Cordillera of the Central Andes: an SRTM DEM based analysis. Geomorphology 139–140:122–135

Kay SM, Coira BL (2009) Shallowing and steepening subduction zones, continental lithospheric loss, magmatism, and crustal flow under the Central Andean Altiplano–Puna plateau. In: Kay SM, Ramos VA, Dickinson WR (eds) Backbone of the Americas: plateau uplift, shallow subduction, and ridge collision. Geol Soc Am Mem 204:229–259. https://doi.org/10.1130/2009.1204(11)

Kay SM, Mpodozis C (2002) Magmatism as a probe to the Neogene shallowing of the Nazca plate beneath the modern Chilean flatslab. J S Am Earth Sci 15:39–59

Kay SM, Coira B, Mpodozis C (2006) Late Neogene volcanism in the Cerro Blanco region of the Puna Austral, Argentina (~26.5°S, ~67.5°W). XI Cong Geol Chileno Actas 2:499–502

Kay SM, Coira B, Wörner G, Kay RW, Singer BS (2011) Geochemical, isotopic and single crystal $^{40}Ar/^{39}Ar$ age constraints on the evolution of the Cerro Galán ignimbrites. B Volcanol 73:1487–1511

Kay SM, Mpodozis C, Gardeweg M (2014) Magma sources and tectonic setting of central Andean andesites (25.5–28°S) related to crustal thickening, forearc subduction erosion and delamination. In: Gómez-Tuena A, Straub SM, Zellmer GF (eds) Orogenic andesites and crustal growth, vol 385. Geol Soc London Spec Publ, pp 303–334

Klemetti EW, Grunder AL (2008) Volcanic evolution of Volcán Aucanquilcha: a long-lived dacite volcano in the Central Andes of northern Chile. B Volcanol 70:633–650

Kraemer B, Adelmann D, Alten M, Schnurr W, Erpenstein K, Kiefer E, van den Bogaard P, Görler K (1999) Incorporation of the Paleogene foreland into the Neogene Puna plateau: the Salar de Antofalla area, NW Argentina. J S Am Earth Sci 12:157–182

Le Maitre RW, Bateman P, Dudek A, Keller J, Lameyre J, Le Bas MJ, Sabine PA, Schmid R, Sørensen H, Streckeisen A, Woolley AR, Zanettin B (1989) A classification of igneous rocks and glossary of terms. Blackwell, Oxford

Lewis-Kenedi CB, Lange RA, Hall CM, Delgado-Granados H (2005) The eruptive history of the Tequila volcanic field, western Mexico: ages, volumes, and relative proportions of lava types. B Volcanol 67: 391–414

Loughlin SC, Vye-Brown C, Sparks RSJ, Brown SK, Barclay J, Calder E, Cottrell E, Jolly G, Komorowski J-C, Mandeville C, Newhall C, Palma J, Potter S, Valentine G (2015) An introduction to global volcanic hazard and risk. In: Loughlin SC, Sparks RSJ, Brown SK, Jenkins SF, Vye-Brown C (eds) Global volcanic hazards and risk. Cambridge University Press, Cambridge, pp 1–79

Matsumoto A, Kobayashi T (1995) K–Ar age determination of late Quaternary volcanic rocks using the "mass fractionation correction procedure": application to the Younger Ontake volcano, central Japan. Chem Geol 125:123–135

Matteini M, Mazzuoli R, Omarini R, Cas R, Maas R (2002) Geodynamical evolution of Central Andes at 24 S as inferred by magma composition along the Calama–Olacapato–El Toro transversal volcanic belt. J Volcanol Geotherm Res 118:205–228

McNutt SR (1996) Seismic monitoring and eruption forecasting of volcanoes: a review of the state-of-the-art and case histories. In: Scarpa R, Tilling RI (eds) Monitoring and mitigation of volcano hazards. Springer-Verlag, Berlin, pp 99–146

Montero López MC, Hongn F, Brod A, Seggiaro R, Marrett R, Sudo M (2010) Magmatismo ácido del Mioceno Superior-Cuaternario en el área de Cerro Blanco-La Hoyada, Puna Austral. Rev Asoc Geol Argent 67:329–348

Mpodozis C, Cornejo P, Kay SM, Tittler A (1995) La Franja de Maricunga: síntesis de la evolución del frente volcánico oligoceno-mioceno de la zona sur de los Andes Centrales. Rev Geol Chile 22: 273–314

Mpodozis C, Kay SM, Gardeweg M, Coira B (1996) Geología de la región de Ojos del Salado (Andes Centrales, 27° S): implicancias de la migración hacia el este del frente volcánico Cenozoico Superior. XIII Cong Geol Arg Actas 3:539–548

Muir DD, Barfod DN, Blundy JD, Rust AC, Sparks RSJ, Clarke KM (2015) The temporal record of magmatism at Cerro Uturuncu, Bolivian Altiplano. In: Caricchi L, Blundy JD (eds) Chemical, physical and temporal evolution of magmatic systems. Geol Soc London Spec Pub 422:57–84

Nagao K, Ogata A, Miura Y, Matsuda J, Akimoto S (1991) Highly reproducible 13 and 17 ka K–Ar ages of two volcanic rocks. Geochem J 25:447–451

Nagao K, Ogata A, Miura YN, Yamaguchi K (1996) Ar isotope analysis for K-Ar dating using two modified-VG5400 mass spectrometers–I: isotope dilution method. J Mass Spectrom Soc Jpn 44:36–61

Naranjo J, Cornejo P (1992) Hoja Salar de la Isla (Escala 1:250.000). Servicio Nacional de Geologia y Mineria de Chile

Norini G, Báez W, Becchio R, Viramonte J, Giordano G, Arnosio M, Pinton A, Groppelli G (2013) The Calama–Olacapato–El Toro fault system in the Puna plateau, Central Andes: geodynamic implications and stratovolcanoes emplacement. Tectonophysics 608: 1280–1297

Ochi Ramacciotti ML, Escalante Fochi F, Grosse P (2017) Volcanismo monogenético máfico cuaternario sobre el lineamiento Peinado, Puna Sur. XX Cong Geol Argentino, Abstract ST8:144–149

Orihashi Y, Naranjo JA, Motoki A, Sumino H, Hirata D, Anma R, Nagao K (2004) The Quaternary volcanic activities of Hudson and Lautaro volcanoes, Chilean Patagonia: new constraints from K–Ar ages. Rev Geol Chile 37:204–224

Ownby S, Delgado Granados H, Lange RA, Hall CM (2007) Volcán Tancítaro, Michoacán, Mexico, $^{40}Ar/^{39}Ar$ constraints on its history of sector collapse. J Volcanol Geotherm Res 161:1–14

Peccerillo R, Taylor SR (1976) Geochemistry of Eocene calcalkaline volcanic rocks from the Kastamonu area, northern Turkey. Contrib Mineral Petrol 58:63–81

Petrinovic IA, Riller U, Brod JA, Alvarado G, Arnosio M (2006) Bimodal volcanism in a tectonic transfer zone: evidence for tectonically controlled magmatism in the southern Central Andes, NW Argentina. J Volcanol Geotherm Res 152:240–252

Polanco E, Clavero J, Arcos R (2014) Cadena Volcánica Los Cuyanos-Sierra Nevada: geoquímica y edades Ar/Ar, Zona Volcánica Central, Región de Atacama, Chile (26°26'S). XIX Cong Geol Arg Actas S24–3-16

Prambada O, Arakawa Y, Ikehata K, Furukawa R, Takada A, Wibowo HE, Nakagawa M, Kartadinata MN (2016) Eruptive history of Sundoro volcano, Central Java, Indonesia since 34 ka. B Volcanol 78:81

Richards JP, Villeneuve M (2001) The Llullaillaco volcano, Northwest Argentina: construction by Pleistocene volcanism and destruction by sector collapse. J Volcanol Geotherm Res 105:77–105

Richards JP, Villeneuve M (2002) Characteristics of late Cenozoic volcanism along the Archibarca lineament from Cerro Llullaillaco to Corrida de Cori, Northwest Argentina. J Volcanol Geotherm Res 116:161–200

Richards JP, Ullrich T, Kerrich R (2006) The late Miocene–Quaternary Antofalla volcanic complex, southern Puna, NW Argentina: protracted history, diverse petrology, and economic potential. J Volcanol Geotherm Res 152:197–239

Riller U, Petrinovic I, Ramelow J, Strecker M, Oncken O (2001) Late Cenozoic tectonism, collapse caldera and plateau formation in the Central Andes. Earth Planet Sc Lett 188:299–311

Risse A, Trumbull RB, Coira B, Kay SM, van den Bogaard P (2008) $^{40}Ar/^{39}Ar$ geochronology of mafic volcanism in the back-arc region of the southern Puna plateau, Argentina. J S Am Earth Sci 26:1–15

Robin C, Samaniego P, Le Pennec JL, Fornari M, Mothes P, van der Plicht J (2010) New radiometric and petrological constraints on the evolution of the Pichincha volcanic complex (Ecuador). Bull Volcanol 72:1109–1129

Rodríguez I, Roche O, Moune S, Aguilera F, Campos E, Pizarro M (2015) Evolution of Irruputuncu volcano, Central Andes, northern Chile. J S Am Earth Sci 63:385–399

Salfity JA (1985) Lineamientos transversales al rumbo Andino en el noroeste Argentino. IV Cong Geol Chileno Actas 2:119–137

Samaniego P, Barba D, Robin C, Fornari M, Bernard B (2012) Eruptive history of Chimborazo volcano (Ecuador): a large, ice-capped and hazardous compound volcano in the northern Andes. J Volcanol Geotherm Res 221:33–51

Samaniego P, Valderrama P, Mariño J, van Wyk de Vries B, Roche O, Manrique N, Chédeville C, Liorzou C, Fidel L, Malnati J (2015) The historical (218±14 aBP) explosive eruption of Tutupaca volcano (southern Peru). Bull Volcanol 77:51

Samaniego P, Rivera M, Mariño J, Guillou H, Liorzoud C, Zerathe S, Delgado R, Valderrama P, Scao V (2016) The eruptive chronology of the Ampato–Sabancaya volcanic complex (southern Peru). J Volcanol Geotherm Res 323:110–128

Scaillet S, Guillou H (2004) A critical evaluation of young (near-zero) K–Ar ages. Earth Planet Sci Lett 220:265–275

Scandone R, Bartolini S, Martí J (2016) A scale for ranking volcanoes by risk. Bull Volcanol 78:2

Schmidt ME, Grunder AL (2009) The evolution of North Sister: a volcano shaped by extension and ice in the central Oregon Cascade Arc. Geol Soc Am Bull 121:643–662

Schnurr WBW, Trumbull RB, Clavero J, Hahne K, Siebel W, Gardeweg M (2007) Twenty-five million years of silicic volcanism in the southern central volcanic zone of the Andes: geochemistry and magma genesis of ignimbrites from 25 to 27 °S, 67° to 72 °W. J Volcanol Geotherm Res 266:27–46

Seggiaro R, Hongn F, Folguera A, Clavero J (2006) Hoja Geológica 2769-II Paso de San Francisco (Escala 1:250.000). Servicio Geológico Minero de Argentina

Siebel W, Schnurr WBW, Hahne K, Kraemer B, Trumbull RB, van den Bogaard P, Emmermann R (2001) Geochemistry and isotope systematic of small- to medium-volume Neogene–Quaternary ignimbrites in the southern Central Andes: evidence for derivation from andesitic magma sources. Chem Geol 171:213–217

Siebert L, Simkin T, Kimberly P (2010) Volcanoes of the world, 3rd edn. University of California Press, Berkeley

Singer BS, Thompson RA, Dungan MA, Feeley TC, Nelson ST, Pickens JC, Brown LL, Wulff AW, Davidson JP, Metzger J (1997) Volcanism and erosion during the past 930 k.y. at the Tatara–San Pedro complex, Chilean Andes. Geol Soc Am Bull 109:127–142

Singer BS, Jicha BR, Harper MA, Naranjo JA, Lara LE, Moreno-Roa H (2008) Eruptive history, geochronology, and magmatic evolution of the Puyehue-Cordón Caulle volcanic complex, Chile. Geol Soc Am Bull 120:599–618

Somoza R, Ghidella ME (2012) Late Cretaceous to recent plate motions in western South America revisited. Earth Planet Sc Lett 331–332: 152–163

Sparks RSJ, Francis PW, Hamer RD, Pankhurst RJ, O'Callaghan LO, Thorpe RS, Page R (1985) Ignimbrites of the Cerro Galán caldera, NW Argentina. J Volcanol Geotherm Res 24:205–248

Szakács A (1994) Redefining active volcanoes: a discussion. B Volcanol 56:321–325

Thouret J-C, Finizola A, Fornari M, Legeley-Padovani A, Suni J, Frechen M (2001) Geology of El Misti volcano near the city of Arequipa, Peru. Geol Soc Am Bull 113:1593–1610

Thouret J-C, Rivera M, Wörner G, Gerbe M-C, Finizola A, Fornari M, Gonzales K (2005) Ubinas: the evolution of the historically most active volcano in southern Peru. B Volcanol 67:557–589

Trumbull R, Riller U, Oncken O, Scheuber E, Munier K, Hongn F (2006) The time-space distribution of Cenozoic arc volcanism in the Central Andes: a new data compilation and some tectonic considerations. In: Oncken O, Chong G, Franz G, Giese P, Götze H-J, Ramos V, Strecker M, Wigger P (eds) The Andes—active subduction orogeny. Front Earth Sci 1:29–43. https://doi.org/10.1007/978-3-540-48684-8

Vezzoli L, Tibaldi A, Renzulli A, Menna M, Flude S (2008) Faulting-assisted lateral collapses and influence onshallow magma feeding system at Ollagüe volcano (Central Volcanic Zone, Chile-Bolivia Andes). J VolcanolGeotherm Res 171:137–159

Ward KM, Delph JR, Zandt G, Beck SL, Ducea MN (2017) Magmatic evolution of a cordilleran flare-up and its role in the creation of silicic crust. Nature Sci Rep 7:9047

Wörner G, Hammerschmidt K, Henjes-Kunst F, Lezaun J, Wilke H (2000) Geochronology ($^{40}Ar/^{39}Ar$, K-Ar and He-exposure ages) of Cenozoic magmatic rocks from northern Chile (18-22°S): implications for magmatism and tectonic evolution of the Central Andes. Rev Geol Chile 27:205–240

Zentilli M (1974) Geological evolution and metallogenetic relationships in the Andes of northern Chile between 26° and 29° south. PhD thesis, Queen's University, Kingston, Canada